12 Data Correction Methods

No measurement is ever perfect. Measurement errors and uncertainties are indeed an intrinsic part of the scientific process. Skilled scientists, however, can devise techniques to minimize errors and correct for biases. In this chapter, we discuss the notions of accuracy, precision, and biases, and examine various sources and types of errors in §12.1. We then present, in §12.2, a discussion of specific sources of uncertainties arising in the nuclear sciences. Techniques to unfold detection efficiencies and resolution effects in the measurement of spectra and elementary cross sections are presented in §12.3 while correction techniques relevant for correlation and fluctuation observables are discussed in §12.4.

12.1 Experimental Errors

An experimental error may be defined as the difference between a measured (observed) value and the true value. This of course assumes the observable of interest is meaningfully defined and in fact has a true value. It should be clear, however, that there can be difficulties with this idea. Certain physical quantities such as temperature are defined only in the context of a large number limit. Indeed, while it is meaningful to speak of the temperature of gas consisting of a very large number of molecules, the notion of temperature becomes meaningless in the presence of only one or two particles. Limitations may also arise because of the quantum nature of phenomena. For instance, there is an intrinsic limitation in simultaneously measuring the instantaneous position and momentum of an elementary particle, although it is perfectly sensible to consider the expectation values (i.e., average) of these two observables.

The true value of a physics observable is, of course, unknown a priori otherwise there would be no reason to conduct an experiment. Knowing the error of a measurement is obviously also impossible, and one must then use the language of probability and statistics to estimate both the true value and the error. Properly conducted measurements, with a sound statistical analysis, are thus expected to yield values close to the true value but without guarantee of ever reaching it with infinite precision or accuracy.

The methods of probability and statistics covered in Part I of this book provide meaningful ways to estimate both the true value and error of any measurement. Most modern physical observables of interest, however, are quantities derived from measurements of one or several observable elementary quantities and calculations. Modern experiments (e.g., experiments at the Large Hadron Collider) are rather complex, and the estimation of errors may at first seem a daunting task. Fortunately, here again, the methods of statistics, and

https://doi.org/10.1017/9781108241922.015 Published online by Cambridge University Press

methods for the propagation of errors covered in Part I enable an estimate of the true values as well as errors on the derived quantities. It is thus useful to examine the various types of errors that can arise in an experiment, identify errors that can be reduced or suppressed by careful design of a measurement, and isolate those that are irreducible or depend on the amount of statistics gathered by an experiment.

Measurement errors and uncertainties can occur for a wide variety of reasons including simple mistakes, calculation errors, instrumentation reading error, instrumental or background processes or process noise that interfere with the measurement, as well as the basic stochastic nature of the measurement process. Improper "reading" of a gauge or the output of a measuring device can be greatly reduced by taking humans out of the measurement process and replacing them with robust and reliable sensors whose measurements are read out by automated computing systems. Errors and uncertainties remain nonetheless an intrinsic part of the experimental process. Indeed, even if human error can be avoided, there remain intrinsic uncertainties associated with physical processes and sensor technologies used to carry out measurements.

Consider, for instance, the identification of particle species in a magnetic spectrometer based on the energy loss (and momentum loss) particles undergo as they traverse sensing devices (see §8.3.3). By its very nature, the collisional processes that leads to energy deposition in a finite thickness sensor is stochastic. Measurement of position and energy loss (and deposition) consequently yield random values according to some PDF determined by the physics of the process (e.g., collisions) and the sensing device. As another example, consider measurements of particle time-of-flight with photosensitive devices, as described in §8.4.2. Particles passing through a material collide with electrons of the material and produce random molecular excitations that result in fluorescence. Timing measurements are obtained when the light collected produces an electronic signal that exceeds a "firing" threshold. The stochastic nature of the photon production and collection processes lead to irreducible fluctuations of the time when the firing threshold is reached and thus result in intrinsic timing uncertainties. The collection of finitely many ions or electrons in energy-sensing devices (such as calorimeters, pad chambers, and so on) similarly result in intrinsic uncertainties. In essence, all techniques relying on the counting of electrons, photons, or other types of particles are fraught with intrinsic uncertainties associated with the stochastic nature of the counting process. Such uncertainties may be mitigated by careful optimization of the detector design to yield a large number of counted particles, better collection, low noise amplification, and so forth, but they can never be eliminated. These sources of stochastic noise are commonly known as **measurement noise**.

Additional uncertainties also arise due to the physics of the detection or measurement process. For instance, measurements of particle momenta in a spectrometer rely on a precise determination of the radius of curvature of charged particle trajectories. The curvature may, however, be stochastically modified when particles pass through the various measuring devices used to establish their trajectory through the spectrometer. Limitations may also occur due to the dual nature of particles and light. The angular resolution of a telescope is, for instance, intrinsically limited by the diffraction of light and the counting of photons in the telescope's focal plane. Although diffraction effects can be suppressed by building increasingly large mirrors, they can never be completely eliminated. Likewise, the

https://doi.org/10.1017/9781108241922.015 Published online by Cambridge University Press

number of photons emitted by a star is finite, and ever increasing aperture sizes can reduce, but never eliminate, the stochastic noise of the photon collection process. In essence, the process used to measure a physical observable also limits the precision and accuracy that can be achieved in any given experiment. Uncertainties associated with the measurement process are usually referred to as **process noise**.

While measurement and process noises cannot be eliminated, careful experimental design can suppress their impact on the outcome of measurements and their uncertainties. It is also possible to handle series of measurements to partially filter out noise effects and obtain optimal treatment of process and measurement noises using the technique known as Kalman filter, already introduced in §5.6.

While measurement errors can be associated with a wide variety of causes and find an irreducible origin in measurement and process noises, one can in general categorize errors and uncertainties into two distinct classes. Errors associated with the randomness of the physical and measurement process are known as **statistical errors**, while those associated with uncertainties in the measurement protocol or method are referred to as **systematic errors**.

Statistical errors refer to the notion that repeated measurements of a given physical quantity yield different values with a "seemingly" random pattern. The randomness arises from the stochastic nature of the measurement and process noise discussed earlier. The random character of the measurement process can usually be described with a probability density function expressing the likelihood of measuring specific values or range of values. Statistical errors can be evaluated, characterized, and reported using the statistical methods discussed in Part I of this book. It is usually safe to assume that measured values are distributed with Poisson or Gaussian probability distributions about their true value, but important deviations from these distributions are also known to occur. Indeed, in practice, errors may "not" alway be perfectly Gaussian.

Systematic errors refer to the notion that a measurement may deviate from the true value because of the measurement method or protocol used to carry out the measurement or the statistical estimator used to in the determination of the observable. The error arises from the system or structure of the measurement technique or apparatus and is thus said to be **systematic**. Systematic errors may arise for various reasons such as instrumentation "reading error," flawed protocol, incorrect experimental model, improper correction methods, or a biased estimator.

Since the true value of an observable is not known, one cannot, by definition, determine the true error. One is thus reduced to estimating error(s) on the basis of our understanding of the measurement (measurement model), prior measurements, fundamental theories (although strictly speaking, measurements are tests of the theories, not the converse), or statistical estimates obtained by comparing several distinct measurements. It is useful to distinguish notions of **accuracy** and **precision**. The former is generally used to describe how close the result of an experiment approaches the true value of an observable, while the latter is used to ascribe how exact a result is obtained without particular reference to the unknown true value. A measurement is generally considered precise if repeated instances of the measurement yield tightly clustered values, that is, values with a small variance. A precise measurement may, however, suffer from biases and systematically deviate from the

https://doi.org/10.1017/9781108241922.015 Published online by Cambridge University Press

true value. It is then considered inaccurate. Conversely, a measurement protocol can be accurate in the sense that it yields results with zero bias but nonetheless remains imprecise because repeated measurements have a large variance. One thus wishes for measurements that are both precise and accurate, that is, with minimal variance and zero bias.

Biases can be introduced either by the **statistical estimators** used in the analysis of data (defined in §4.3) or from the experimental procedure used to carry out the measurement. For instance, a raw measurement of cross section is intrinsically biased since particle detection can never be accomplished with perfect efficiency. It is thus necessary to correct for such inefficiencies. As we shall see in §12.3, while correction methods used to account for limited detection efficiency may in principle be unbiased, practical considerations often limit the estimation of biases and errors, and one must estimate systematic uncertainties. It is important to note that estimation of systematic uncertainties is by far the most challenging component of error estimation. While there is no single or unique method to estimate systematic uncertainties, it is nonetheless possible to formulate generic principles and guidelines, which we discuss in §12.5.

It is also useful to distinguish between absolute and relative uncertainties or errors. Absolute error refers to the actual size of errors expressed in the same units as the actual measurement. For instance, the measurement of the length of a 1-meter rod could have an absolute uncertainty of 0.001 m. That is, the length is known up to a precision of 0.001 m. Repeated measurements of length are expected to cluster around the expectation value of 1 m with a standard deviation of 0.001 m. A relative error indicates the size of an error relative to the magnitude of the observable and is typically expressed as a percent error obtained by multiplying by 100 the ratio of the uncertainty by the expectation value of the observable (magnitude). The notion of relative error is particularly useful for the description of elementary particle production cross sections. Indeed, since particle production cross sections may have very large ranges of values (from femtobarns to barns), stating the error on a cross section in barns (or any subunits) is thus not particularly informative. Errors on cross sections are thus often reported in terms of relative errors.

The precision of a measurement is obviously manifest if the error is reported. But it is also evident in the number of **significant figures** used to report the measured value. **Significant figures** (also called significant digits) are those digits that carry meaning contributing to the precision of a number. Significant figures exclude all leading zeros or trailing zeros used as placeholders to indicate the scale of a number, as well as spurious digits introduced, for example, by calculations carried out to greater precision than that of the original data, or measurements reported to a greater precision than the equipment supports. By convention, if there is no digital point, the rightmost nonzero digit is the least significant digit. However, if there is a decimal point the rightmost digit is considered as the least significant digit even if zero. All digits between the least and most significant digits are counted as significant (see examples in Figure 12.1).

Use of the **normalized scientific notation** is strongly recommended to report all scientific results and avoid ambiguities on the number of significant figures. In the scientific notation, all numbers are written in the form $a \times 10^b$, where the exponent b is an integer and the coefficient a a real number. The exponent b is chosen so that the absolute value

https://doi.org/10.1017/9781108241922.015 Published online by Cambridge University Press

3.142	0.3142	0.003142
2.718×10^{-5}	$2.718 \times 10^{+7}$	2718000
5.000	500.0	5000.

Fig. 12.1 All numbers shown have four **significant figures**.

of a lies in the range $1 \leq |a| \leq 10$. Thus 15600 is written as 1.56×10^4 while 230000. is denoted 2.30000×10^5. This form allows easy identification of the number of significant figures and comparison of numbers, because the exponent b gives the number's order of magnitude. The exponent b is negative for a number with absolute value between 0 and 1. For instance, 0.50 should be written as 5.0×10^{-1}. The 10 and its exponent are usually omitted when $b = 0$.

When quoting results, the number of significant figures should be approximately one more than that dictated by the experimental precision. This is useful mainly for calculation purposes, since it avoids illegitimate loss of precision in calculations. Additionally, when insignificant digits are dropped from a number, the last digit should be rounded off for best accuracy. One should truncate and treat excess digits as decimal fractions. The least significant digit should be incremented by one unit if the fraction is greater than $1/2$, or if the fraction equals $1/2$ and the least significant digit is odd.

As discussed earlier, statistical and systematic uncertainties have quite different origins and make different statements about the reliability of a measured value. It is thus common practice to report the two uncertainties explicitly and separately. For instance, if the measured cross section of a process is 240 mB with a statistical precision of 24 mB and a systematic uncertainty of 30 mB, one shall report the measurement as

$$240 \pm 24(stat) \pm 30(sys)\ \text{mB}, \tag{12.1}$$

in which the labels "stat" and "sys," which stand for *statistical* and *systematic*, respectively, are often omitted. As we already discussed in Part I of this book, the usual practice is to report one sigma (1σ) statistical uncertainties (whether based on the frequentist or Bayesian paradigms) but greater significance levels are occasionally used and identified as such.

The aforementioned notation implies the errors are symmetric, in other words, that it is equally probable that the true value of an observable be found below or above the quoted value and in the given range. It is often the case, however, that the confidence interval is in fact not symmetric about the quoted value. This may occur, for instance, when an observable A is obtained from a one parameter fit to some data. In this case, a 1σ interval should be determined by the range of the fitted parameter which, relative to the parameter value a at the minimum χ^2_{min}, yields a χ^2 increase of one unit. As schematically illustrated in Figure 12.2, if the χ^2 function, plotted vs. the fit parameter, is not symmetric relative to its minimum, the low-side range, $\Delta a_<$, and high-side range, $\Delta a_>$, required to produce a χ^2 increase of one unit are not equal. The uncertainty interval is thus asymmetric and is usually reported according to the low/high notation. One would, for instance, write

$$240^{+20}_{-6}\ \text{mB}. \tag{12.2}$$

https://doi.org/10.1017/9781108241922.015 Published online by Cambridge University Press

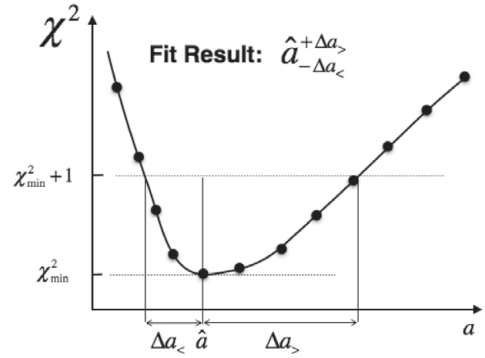

Fig. 12.2 Schematic illustration of conditions under which asymmetric error intervals are obtained from $\mathbb{LS}$ fits. The χ^2 function is plotted, for a given dataset, as a function of a model parameter "a." A one sigma error corresponds to the range in which the χ^2 increases by one unit relative to its minimum value. Given the dependency of χ^2 on a is asymmetric, one must quote the ranges $\Delta a_<$ and $\Delta a_>$ as low- and high-side errors, respectively, as shown.

Asymmetric error intervals may also occur in multiparameter fits or when the measured value is close to a physical boundary (see, e.g., §6.1.8). Asymmetric error intervals are also often reported for systematic errors. Indeed, it is quite possible that the measurement protocol might have a "one-side" effect on an observable, or that the effect is more prominent on the low- or high-side of the reported value. It is thus common to report low- and high-side intervals for both statistical and systematic uncertainties as follows

$$240^{+20}_{-6}(\text{stat})^{+33}_{-22}(\text{sys})\ \text{mB}. \tag{12.3}$$

There is no universally adopted standard notation or method to report errors in graphs. However, in physics, most particularly in high-energy physics, it has essentially become the norm to report statistical and systematic errors independently. Statistical errors are usually indicated with a simple vertical line (for the error on the dependent variable) passing through the data point it qualifies and the length of which corresponds to the size of the confidence interval. Some authors like to terminate the vertical line at both extremities with a short horizontal segment, but this practice has become rather infrequent in the last decade or so. Systematic errors are reported using a wide variety of notations and techniques depending on the circumstances and complexity of the data and errors. Some of these notations are schematically illustrated in Figure 12.3.

12.2 Experimental Considerations

All measurements of physical observables are subjected to limitations, constraints, and alterations associated with the nature of the measurement process as well as the properties

https://doi.org/10.1017/9781108241922.015 Published online by Cambridge University Press

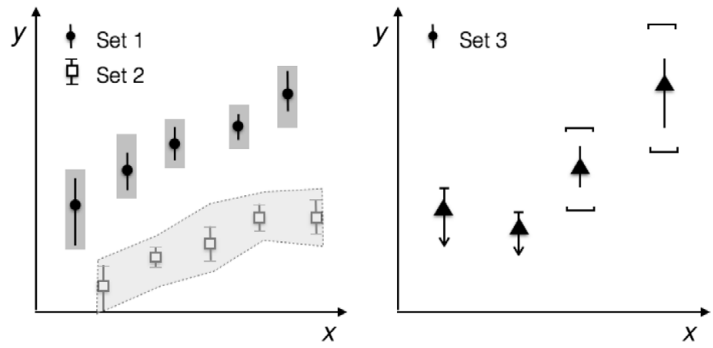

Fig. 12.3 Schematic illustration of notations and techniques commonly used for reporting errors in graphs displaying experimental results. Statistical error bars are shown with solid vertical lines. Error bars with downward pointing arrows are used to represent one-sided confidence levels with an upper limit. Systematic errors are shown with gray boxes for set 1, a shaded range for set 2, and brackets for set 3.

of the apparatus or devices used to carry them. These effects can be broadly categorized in terms of the following:

1. Experimental acceptance
2. Detection efficiency
3. Smearing and resolution
4. Ghost and background signals

Let us briefly discuss each of these effects.

12.2.1 Acceptance

The **acceptance** of a measurement corresponds to the range in which an observable of interest can be measured. The determination of the acceptance of a measurement is often a trivial matter, but it can also be rather complicated. At a basic level, the acceptance is determined by the device carrying out the measurement and the range in which an elementary observable is acquired. For instance, when measuring the time-of-flight (TOF) of particles, one is typically limited by the physical scale of the apparatus and the specific time-to-digital converter (TDC) used to carry out the time-to-digital conversion. The acceptance may also be determined by the measurement process itself. Consider, for instance, the measurement of the momentum of charged particles in a magnetic spectrometer. The momentum is proportional to the radius of the charged particle trajectories and the magnetic field. If the momentum of the particles is too small, their trajectory might not be measurable by the sensing devices and they will simply be lost, that is, not accepted in the measurement. The acceptance associated with certain measurements can be rather complex and depend both on the physical process involved and the measurement itself. This is particularly the case when the measurement process involves a cascade of different phenomena. For

https://doi.org/10.1017/9781108241922.015 Published online by Cambridge University Press

instance, the detection of a Higgs boson decaying into jets requires that one detects the jets, which in turn requires that one detects the charged and neutral particles of these jets. The acceptance of the Higgs is then dependent on several measurement processes and devices.

Given the range of conditions that may constrain the acceptance of a specific measurement, the actual determination of the acceptance may become an arduous task that is typically best carried out by modeling the measurement process and instruments by Monte Carlo simulations. We will consider selected illustrative examples in Chapter 14.

The acceptance of a measurement effectively defines the range of its applicability. Measured observables can be genuinely reported only if they are within the acceptance of the measurement. They thus cannot be corrected, strictly speaking, for unmeasured ranges of values. However, if there are observables whose behavior can be predicted with good certainty outside a measurement of interest (e.g., production cross section of particles vanishes at zero and infinite momentum), it may then be possible to carry out reliable extrapolations of the measurements, sometimes referred as **acceptance corrections**. It should be clear that such "corrections" are extrapolations whose validity and accuracy depend on the specificities of the observables and the measurement itself.

12.2.2 Efficiency

Whether one conducts a measurement of an elementary physical quantity (i.e., the amplitude of a magnetic field) or a more elaborate observable (e.g., the production cross section of a specific type of particle), one is invariably faced with the fact that some "events" will be lost either because of the nature of the phenomenon and observable being measured, that is, the process, or because of the measurement device itself. Consider, for instance, the detection of charged pions in a magnetic spectrometer. Since charged pions decay with a mean lifetime of 2.6×10^{-8} s, a substantial fraction may be lost because they decay in flight through the apparatus and consequently do not produce any or sufficient signals in sensing devices. Pions may also be lost because of various effects arising in the detection process such as fluctuations in energy deposition, charge collection, electronic noise, detector component malfunction, and so on.

The **efficiency**, ϵ, of a measurement is generically defined as the ratio of the expectation value of the number of measured "events," $\langle N_M \rangle$, by the expectation value of the number of produced (or true) events, $\langle N_T \rangle$:

$$\epsilon = \frac{\langle N_M \rangle}{\langle N_T \rangle}. \tag{12.4}$$

The word *event* refers to instances or occurrences of a particular phenomenon of interest, such as supernova explosions, proton–proton collisions, or the production of charged particles.

Methods for efficiency correction of spectra and correlation functions are presented in §§12.3 and 12.4.3, respectively, whereas techniques to determine the efficiency of measurements are discussed in §§12.4.6 and 14.2.4.

https://doi.org/10.1017/9781108241922.015 Published online by Cambridge University Press

12.2.3 Signal Smearing, Precision, and Resolution

Strictly speaking, **signal smearing** refers to the notion that the **precision** of a measurement of a physical observable is invariably finite, while the term **resolution**, often called **resolving power**, corresponds to the ability of a particular measurement to distinguish or separate two "close-by" signals, phenomena, or entities, e.g., two peaks in a frequency or mass spectrum. In practice, the term resolution is often misused to refer to both precision and separation of close-by signals. As for acceptance and efficiency, both physical processes and the properties of a device have an influence on the **precision** and **resolution** of the measurement.

Consider, for instance, the measurement of the momentum of charged particles with a magnetic spectrometer, where the momentum is determined based on the radius of curvature of the charged particle trajectories. As they traverse detector components, scatterings with electrons and nuclei of the medium change their momentum and direction randomly. The radii and directions of the tracks are consequently randomly altered and yield a smearing of the measured momenta, and thus a **loss of precision**. Signal smearing also arises from the technique used to extract the radius of curvature. One must be able to sample hits or points where particles traverse specific components of the apparatus. Devices used to measure these points have finite granularity and feature finite signal-to-noise characteristics. They thus yield position measurements of finite precision, which in turn produce smearing, or **loss of precision**, in the determination of the radius of curvature of the charged particle tracks. The momentum of measured charged particles is thus limited by both scattering processes and the precision of hit measurements. This is true of all observables in general.

Process noise and measurement noise also limit the **resolving power** of a measurement. Consider once again the measurement of charge particles in a detector. Charged particles passing through a sensing device lose energy as they scatter with electrons and nuclei of the material. This lost energy is used to produce a signal and detect the passage of the particle. But, based on the need to collect the lost energy to produce a signal (often in terms of the amount of ionization produced by the particle), the sensing device must have a finite area. There can also be energy or signal sharing between nearby sensing units. This implies that the signals produced by the passage of two particles through a given detection unit may not be separable as two distinct signals and that they may then be confused as a single signal. The term resolution thus typically refers to the minimum signal separation (in the observable's units) required to reliably separate two distinct signals.

Process and measurement smearing, or noise, may be described, typically, in terms of a response function, $r(x_m|x_t)$, expressing the probability of obtaining a specific measured value, x_m, given an actual or true value, x_t. This response can in principle be expressed in terms of a well-defined PDF, with unit normalization:

$$\int_{\text{accept}} r(x_m|x_t)\, dx_m = 1. \tag{12.5}$$

The accuracy and precision of a measurement can be reported either in terms of its response function, if it is explicitly known, or in terms of its (estimated) moments. The first and

https://doi.org/10.1017/9781108241922.015 Published online by Cambridge University Press

second moments of $r(x_m|x_t)$ determine the bias and the accuracy of the measurement. The bias is obtain from the first moment

$$B_x \equiv \langle x_m \rangle - x_t = \int_{\text{accept}} (x_m - x_t)\, r(x_m|x_t)\, dx_m \tag{12.6}$$

whereas the accuracy is appraised on the basis of its mean square error (MSE).[1]

$$\text{MSE} = \left(\int_{\text{accept}} (x_m - x_t)^2\, r(x_m|x_t)\, dx_m \right)^{1/2}. \tag{12.7}$$

As already discussed in §4.4, the MSE depends on the bias B_x and the variance σ_x^2 of the measured value x_m (an estimator of x_t which in the context of §4.4 would be denoted $\hat{x}$) relative to its expectation value, $\langle x_m \rangle = E[x_m]$. The accuracy of the measurement may then be written

$$\text{MSE} = B_x^2 + \sigma_x^2, \tag{12.8}$$

where $\sigma_x^2 = E\left[(x_m - E\,[x_m])^2\right]$. Effectively, MSE provides an assessment of the overall accuracy of the measurement influenced in part by the bias B_x and the standard deviation σ_x of the measured value one would observe if the same experiment could be repeated several times.

The response function $r(x_m|x_t)$ can often be approximated with a Gaussian distribution. This is "guaranteed" by the central limit theorem, in particular, when the measurement outcome is a sum or superposition of several subprocesses. Examples of such processes include measurements of the energy of elementary particles with calorimeters, measurements of the curvature of tracks in a magnetic spectrometer, and the determination of particles' TOF with TOF detectors. However, $r(x_m|x_t)$ may also drastically deviate from a Gaussian distribution and feature long tails or various substructures. This is the case, for instance, of measurements of the energy loss of charged particles traversing a time projection chamber where scatterings can lead to large energy losses, or in the detection and measurement of the energy of jets where loss of particles (because of detection efficiencies) can lead to large amounts of missing jet energy.

The response $r(x_m|x_t)$ may be a rather complex function of intrinsic and extrinsic conditions. For instance, the transverse momentum resolution of a charged particle track typically depends on the actual momentum of the particle, its angle of emission (production), and its rapidity. It may also depend on detector-wide or event conditions. For instance, since the occupancy of a detector may influence the noise generated within the detector and the pattern recognition involved in finding and obtaining the momentum of tracks, the resolution or response function may then be dependent on such factors as the beam luminosity, the data acquisition rate, and so on.

There are a variety of techniques to determine the precision/resolution of measurements of physical observables. It is often possible to calibrate and measure the resolution of a device by measurements of well-known standards or calibrated inputs, but measurements with complex detectors typically rely on detailed simulations of the physical processes

[1] Technically, it is the MSE of the estimator of the observable of interest that one reports.

https://doi.org/10.1017/9781108241922.015 Published online by Cambridge University Press

involved, as well as the performance of the detector components. Selected techniques used in the estimation of observable resolution and to account (i.e., correct) for finite resolution are discussed in §12.3 of this chapter, whereas basic simulation techniques used to simulate smearing effects are covered in §14.2.

12.2.4 Ghost Signals and Background Processes

Ghost signals refer to noise that may be construed as a signal either because it exceeds a specific measurement threshold or because it is explicitly reconstructed as such. Electronic noise and process noise produce signal fluctuations that occasionally have large amplitude and may thus fake actual signals. This is particularly the case when considering "elementary" observables measured by basic sensor units or detector components. More elaborate ghost signals may also occur as a result of such basic noise signal. For instance, fake tracks may be reconstructed in a spectrometer as a result of noisy electronics, correlated electronic signals, component malfunctions, or by incorrect association of true particle hits.

Background processes may also impede measurements of a particular observable. For instance, combinatorial pairs of particles may contribute a strong background in the reconstruction of the mass spectrum of decaying particles, and secondary particles (resulting from decays within the apparatus) contribute an undesirable background in measurements of particle production cross section and correlation functions.

Techniques to evaluate signal noise and background processes are as varied as the observables measured by scientists. A detailed discussion of such techniques is beyond the scope of this textbook.

12.3 Signal Correction and Unfolding

The problem of unfolding is formally introduced in §12.3.1. Given the intricacies of the unfolding problem, many scientists opt to compare their data to folded theoretical data rather than unfolding their measurements for instrumental effects. The relative merits of this alternative approach and unfolding of the detector effects are briefly discussed in §12.3.3. The correction coefficient method, commonly known as the bin-by-bin technique, and its limitations, are presented in §12.3.4. Actual unfolding techniques, including regularization, are described in §§12.3.6, 12.3.7, and 12.3.8.

12.3.1 Problem Definition

As discussed already in §12.2 of this chapter, measurements of physical observables involve a variety of instrumental effects that must be properly accounted for to obtain robust scientific results. These include effects associated with limited acceptance, detection efficiency, measurement resolution, possible nonlinearities, and the presence of noise and backgrounds. While extrapolation outside of the acceptance of a specific measurement is

https://doi.org/10.1017/9781108241922.015 Published online by Cambridge University Press

not usually warranted, corrections for efficiency, finite resolution, nonlinearities, and background processes are usually possible to perform in a well-controlled manner. Indeed, if an experiment and the observable X it measures are well defined, and if the experimental performance is reasonably stable, it is possible to account for efficiency and resolution effects in a deterministic fashion.

Let us consider a measurement of a specific observable X by a specific apparatus. We will represent by x_t the true value of the observable X, and by x_m the value observed with the apparatus. We will carry out our discussion assuming X is a simple observable (e.g., the transverse momentum, p_T), but the method discussed in the following is trivially extended to multidimensional observables (e.g., $\vec{p} = (p_T, \eta, \phi)$).

Let us first introduce the PDFs of the true, measured, and background distributions. Let $f_t(x_t)$ represent the probability (density) of observing true values x_t, with normalization:

$$\int_{\Omega_t} f_t(x_t)\, dx_t = 1, \tag{12.9}$$

where the integral is taken over the relevant domain Ω_t of the observable X. Likewise, let us denote the PDF of the measured distributions by $f_m(x_m)$, with similar normalization.

$$\int_{\Omega_m} f_m(x_m)\, dx_m = 1. \tag{12.10}$$

In general, the measured distribution f_m may involve a superposition of the true but smeared signal and some background. We will denote the PDF of this background as $f_b(x_m)$ and use the normalization

$$\int_{\Omega_m} f_b(x_m)\, dx_m = 1. \tag{12.11}$$

We will assume that it is possible, experimentally, to determine both the shape of this background PDF as well as the relative rate of background events.

If several background processes and sources of noises hamper the measurement, one can include them by estimating their respective distributions. Let us define p_α as the relative probability of a specific background process α and assume one can describe its distribution of measured values x_m in terms of a PDF, $f_{b,\alpha}(x_m)$, which represents the probability of measuring x_m given the background process α. The probability of observing values x_m produced by N_α background processes may then be written

$$f_b(x_m) = \sum_{\alpha=1}^{N_\alpha} p_\alpha f_{b,\alpha}(x_m), \tag{12.12}$$

where we require, by definition,

$$\int_{\Omega_m} f_{b,\alpha}(x_m)\, dx_m = 1, \tag{12.13}$$

$$\sum_{\alpha=1}^{N_\alpha} p_\alpha = 1.$$

https://doi.org/10.1017/9781108241922.015 Published online by Cambridge University Press

We define the experimental response function, noted $R(x_m|x_t)$, as the probability (density) to observe a value x_m when the "event" has value x_t. This response function has two components:

$$R(x_m|x_t) = r(x_m|x_t) \times \epsilon(x_t). \tag{12.14}$$

The coefficient $r(x_m|x_t)$ is the smearing function of the measurement. It is determined by process noises and measurement noises, as briefly discussed in §12.2.4. It is a PDF representing the probability of finding a value x_m when the true value is x_t. By construction, one has the normalization

$$\int_{\Omega_m} r(x_m|x_t)\, dx_m = 1, \tag{12.15}$$

where Ω_m represents, here again, the domain of the measured values x_m.

The function $\epsilon(x_t)$ represents the efficiency of the measurement and thus corresponds to the probability of actually observing an "event" with an observable value x_t. Similarly to $r(x_m|x_t)$, the efficiency $\epsilon(x_t)$ may depend both on properties of the measurement process (e.g., decays typically reduce the efficiency of observing particles) and characteristics or performance of the apparatus. This could be, for instance, the probability of detecting charged particles within a magnetic spectrometer as a function of their transverse momentum, or the probability of finding and reconstructing a given type of collision at a proton collider.

In general, the functions $r(x_m|x_t)$ and $\epsilon(x_t)$ may have dependencies on other variables such as external or global conditions of the apparatus and collisions being measured. For example, both the efficiency and the smearing function of charged particle measurement usually depend on their direction (rapidity, azimuth angle), as well as the complexity of the events of which they are part of, the detector occupancy, the data acquisition rate, and so on.

Experimentally, given finite statistics and resolution, it is convenient to discretize the true, measured, and background distributions using histograms $\vec{\mu} = (\mu_1, \mu_2, \ldots, \mu_M)$, $\vec{\nu} = (\nu_1, \nu_2, \ldots, \nu_N)$, $\vec{\beta} = (\beta_1, \beta_2, \ldots, \beta_N)$. In general, the true and measured histograms may have different number of bins, M and N, as well as different ranges. We will see later in this section how these differences may impact the determination of the true distribution in practice.

Let us denote the number of true, measured, and background events observed in a given experiment by m_{tot}, n_{tot}, and b_{tot}, respectively. Their expectation values are

$$\mu_{\text{tot}} = \mathrm{E}\left[m_{\text{tot}}\right], \tag{12.16}$$

$$\nu_{\text{tot}} = \mathrm{E}\left[n_{\text{tot}}\right], \tag{12.17}$$

$$\beta_{\text{tot}} = \mathrm{E}\left[b_{\text{tot}}\right]. \tag{12.18}$$

We will show in the following that the number of measured events shall be equal to

$$\nu_{\text{tot}} = \langle\epsilon\rangle \mu_{\text{tot}} + \beta_{\text{tot}}, \tag{12.19}$$

where $\langle\epsilon\rangle$ represents the average efficiency of the measurement. We will assume it is possible to determine β_{tot} unambiguously, although this may prove to be challenging in practice.

https://doi.org/10.1017/9781108241922.015 Published online by Cambridge University Press

The probability, p_j, of x_t being "produced" in bin j is the integral of the PDF $f_t(x_t)$ across that bin:

$$p_j = \int_{\text{bin } j} dx_t f_t(x_t). \tag{12.20}$$

The expectation value of the number of entries in bin j of the true value histogram is thus

$$\mu_j = \mu_{\text{tot}} \times p_j = \mu_{\text{tot}} \int_{\text{bin } j} dx_t f_t(x_t). \tag{12.21}$$

Likewise, the expectation value of the number of entries in bin i of the measured and background distributions shall be

$$\nu_i = \nu_{\text{tot}} \int_{\text{bin } i} dx_m f_m(x_m), \tag{12.22}$$

$$\beta_i = \beta_{\text{tot}} \int_{\text{bin } i} dx_m f_b(x_m). \tag{12.23}$$

Evidently, the number of entries ν_i is a superposition of the smeared true signal, including the detection efficiency and fake signals from background processes. First ignoring backgrounds, one can write

$$\nu_i = \mu_{\text{tot}} \times \text{Probability(event in bin } i). \tag{12.24}$$

The probability of having an event in bin i is determined by the product of the smearing function $R(x_m|x_t)$ and the PDF $f_t(x_t)$. One can thus write

$$\begin{aligned} \nu_i &= \mu_{\text{tot}} \int_{\Omega_t} dx_t \text{Prob}(x_m \text{ in } i|\text{true } x_t, \text{detected}), \\ &\quad \times \text{Prob(detect } x_t) \times \text{Prob(produce } x_t), \end{aligned} \tag{12.25}$$

$$= \mu_{\text{tot}} \int_{\text{bin } i} dx_m \int_{\Omega_t} dx_t r(x_m|x_t)\epsilon(x_t) f_t(x_t). \tag{12.26}$$

The integral over x_t may be partitioned into M bins j by including a sum over all such bins:

$$\nu_i = \mu_{\text{tot}} \int_{\text{bin } i} dx_m \sum_{j=1}^{M} \int_{\text{bin } j} dx_t r(x_m|x_t)\epsilon(x_t) f_t(x_t). \tag{12.27}$$

We seek to express ν_i in terms of the true histogram values μ_j. Multiplying the argument of the integral by $\mu_j/\mu_j = 1$ and rearranging, we get

$$\nu_i = \sum_{j=1}^{M} \int_{\text{bin } i} dx_m \int_{\text{bin } j} dx_t \frac{r(x_m|x_t)\epsilon(x_t) f_t(x_t)}{\mu_j/\mu_{\text{tot}}} \mu_j. \tag{12.28}$$

This may be written

$$\nu_i = \sum_{j=1}^{M} R_{ij}\mu_j, \tag{12.29}$$

https://doi.org/10.1017/9781108241922.015 Published online by Cambridge University Press

with the introduction of the response matrix R_{ij}, defined as

$$R_{ij} = \frac{\int_{\text{bin } i} dx_m \int_{\text{bin } j} dx_t r(x_m|x_t)\epsilon(x_t) f_t(x_t)}{\int_{\text{bin } j} dx'_t f_t(x'_t)}, \tag{12.30}$$

where we used Eq. (12.21) to express the ratio μ_j/μ_{tot}. The numerator of Eq. (12.30) corresponds to the joint probability of measuring a signal in x_m bin i when the true value is in bin j, while the denominator amounts to the probability of finding the true signal in bin j. This ratio is thus the conditional probability of getting a measured signal in bin i when the true signal is in bin j:

$$R_{ij} = \text{Prob}(\text{observed in bin } i|\text{true in bin } j). \tag{12.31}$$

Summing over all observed bins i, one gets

$$\sum_{i=1}^{N} R_{ij} = \epsilon_j, \tag{12.32}$$

where ϵ_j represent the average detection efficiency in bin j:

$$\epsilon_j = \frac{\int_{\text{bin } j} dx_t \epsilon(x_t) f_t(x_t)}{\int_{\text{bin } j} dx_t f_t(x_t)}. \tag{12.33}$$

The expression Eq. (12.29) of the expectation value of the measured signal ν_i is incomplete since we have so far neglected background processes. Assuming the density $f_b(x_m)$ and the number of background events can be reliably estimated, one can write

$$\nu_i = \sum_{j=1}^{M} R_{ij}\mu_j + \beta_i, \tag{12.34}$$

where β_j represents the expectation value of the background processes obtained with Eq. (12.23). This expression can be conveniently represented in terms of a matrix equation as follows:

$$\vec{\nu} = R\vec{\mu} + \vec{\beta}, \tag{12.35}$$

where $\vec{\nu}$ and $\vec{\beta}$ represent $N \times 1$ column vectors, $\vec{\mu}$ is an $M \times 1$ column vector, and R is an $N \times M$ matrix.

The histogram $\vec{\nu}$ represents the expectation value of the measured distribution. In practice, an experiment shall obtain a specific histogram, hereafter noted $\vec{n}$, exhibiting statistical deviations from $\vec{\nu}$. However, repeated measurements of $\vec{n}$ should, on average, converge toward $\vec{\nu}$. Indeed, one should have

$$E[\vec{n}] = \vec{\nu}. \tag{12.36}$$

It thus seems legitimate to replace $\vec{\nu}$ by $\vec{n}$ in Eq. (12.35), and seek an inverse of the matrix R in order to obtain an estimate of $\vec{\mu}$ according to

$$\vec{m} \equiv \hat{\mu} = R^{-1}\left(\vec{n} - \vec{\beta}\right). \tag{12.37}$$

https://doi.org/10.1017/9781108241922.015 Published online by Cambridge University Press

It is relatively straightforward to show that the estimator $\vec{m}$ corresponds to the solution of the least square problem with

$$\chi^2(\vec{\mu}) = \sum_{i,j=1}^{N} (\nu_i - n_i) \left(V^{-1}\right)_{ij} (\nu_i - n_i), \tag{12.38}$$

where ν_i are treated as functions of fit parameters μ_j defined by Eq. (12.34), and the matrix V^{-1} is the inverse of the covariance matrix:

$$V_{ij} = \mathrm{Cov}\left[n_i, n_j\right]. \tag{12.39}$$

Assuming the inverse R^{-1} exists, one finds (see Problem 12.4) that the minimal $\chi^2(\vec{\mu})$ obtained by simultaneously solving

$$\frac{\partial \chi^2(\vec{\mu})}{\partial \mu_k} = 0 \tag{12.40}$$

indeed corresponds to Eq. (12.37). It is also possible to demonstrate that the estimator $\vec{m}$, given by Eq. (12.37), corresponds to the solution obtained by maximization of the log-likelihood function (see Problem 12.7):

$$\log L(\mu) = \sum_{i=1}^{N} \log\left(P(n_i|\nu_i)\right), \tag{12.41}$$

where $P(n_i|\nu_i)$ is a Poisson distribution (or binomial distribution).

The estimator $\vec{m}$, defined by Eq. (12.37), is in fact an unbiased estimator of $\vec{\mu}$:

$$\begin{aligned} \mathrm{E}\left[m_j\right] &= \sum_{i=1}^{N} \left(R^{-1}\right)_{ji} \left(\mathrm{E}\left[n_i\right] - \beta_i\right), \\ &= \sum_{i=1}^{N} \left(R^{-1}\right)_{ji} (\nu_i - \beta_i), \\ &= \mu_j, \end{aligned} \tag{12.42}$$

insofar as the noise spectrum $\vec{\beta}$ is properly estimated.

The covariance between distinct bins of the estimator is calculated similarly and amounts to

$$\mathrm{Cov}\left[m_i, m_j\right] = \sum_{k,k'=1}^{N} \left(R^{-1}\right)_{ik} \left(R^{-1}\right)_{jk'} V_{ij}, \tag{12.43}$$

where V_{ij} is the covariance matrix defined in Eq. (12.39). Defining matrix elements $U_{ij} = \mathrm{Cov}\left[m_i, m_j\right]$, the preceding may be written in the compact form:

$$U = R^{-1} V \left(R^{-1}\right)^T, \tag{12.44}$$

https://doi.org/10.1017/9781108241922.015 Published online by Cambridge University Press

where the label T indicates the transpose of the matrix R^{-1}. If the measured n_i obey Poisson statistics, one has $V_{kk'} = \delta_{kk'} n_k$. The expectation of the covariance matrix U is thus

$$U_{ij} \equiv \mathrm{Cov}\left[m_i, m_j\right] = \sum_{k=1}^{N} \left(R^{-1}\right)_{ik} \left(R^{-1}\right)_{jk} \nu_k, \tag{12.45}$$

from which we conclude that if R is diagonal or nearly diagonal, so should the matrix U.

One can additionally verify that the variance of each component m_j corresponds to the RCF bound obtained with the maximum log-likelihood $\log L(\mu)$. The estimator $\vec{m}$ defined by Eq. (12.37) has zero bias and finite covariance. It should thus provide us, in principle, with a solution to the inverse problem. It should then be possible to correct a measurement for instrumental effects, provided one can invert the response function R. In practice, life is a little more complicated. There are, in fact, several issues with this inverse problem, which we discuss in details in the following section.

12.3.2 Issues with the Inverse Problem...

The first issue encountered with the inverse problem is that the calculation of R requires knowledge of $f_t(x_t)$. This is a problem because this quantity is precisely the answer we seek with our solution of the inverse problem. Indeed, the calculation of the integrals in Eq. (12.30) does require knowledge of f_t. In practice, however, this is only a minor issue because one usually carries out a calculation of the response function $R(x_m|x_t)$ using a MC procedure based on a model PDF, f_{MC}, chosen to be a close approximation of the data. One can then verify by explicit calculations, or by iterative procedures, whether the model f_{MC} enables a reliable estimation of the response matrix R_{ij}. Additionally, it is easy to verify that if $f_t(x_t)$ is approximately constant throughout any given bin j, that it can be factorized out of the integral in x_t and thus cancels out:

$$R_{ij} \approx \frac{f_t(x_{t,j}) \int_{\text{bin } i} dx_m \int_{\text{bin } j} dx_t r(x_m|x_t)\epsilon(x_t)}{f_t(x_{t,j}) \int_{\text{bin } j} dx'_t}, \tag{12.46}$$

$$= \frac{1}{\Delta x_{t,j}} \int_{\text{bin } i} dx_m \int_{\text{bin } j} dx_t r(x_m|x_t), \epsilon(x_t), \tag{12.47}$$

where $\Delta x_{t,j}$ represents the width of bin j.

A far more serious issue with our solution to the inverse problem is that it typically produces wildly oscillating solutions that are not usable in practice. To illustrate this problem, consider the true signal (thick solid line) in Figure 12.4 and the response/smearing function plotted in Figure 14.8. Application (folding) of the smearing function produces the measured expectation value shown in Figure 12.4 as a thin solid line. In an actual experiment, the measured data has finite statistics and exhibit bin-to-bin fluctuations, shown as a dash-line histogram. Unfolding of this measured histogram with Eq. (12.37) unfortunately yields a corrected distribution with large oscillations as illustrated in Figure 12.4 by the solid dots. In spite of all good intents and purposes, this method simply does not work. The unfolded distribution is totally different from the original distribution.

https://doi.org/10.1017/9781108241922.015 Published online by Cambridge University Press

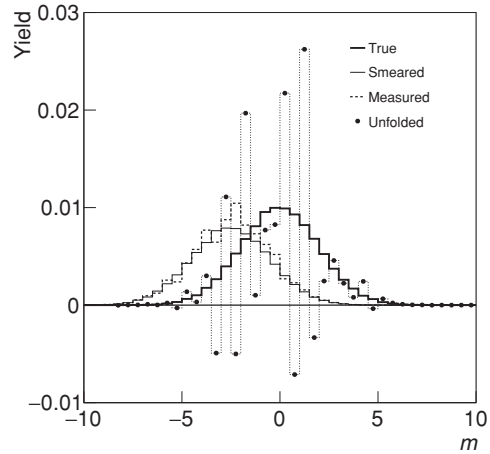

Fig. 12.4 Unregularized unfolding is inherently unstable because the procedure attempts to unsmear peaks and consequently yield spiky structures for spectra with finite statistics.

The failure is no mere numerical instability or coding error. It is an intrinsic feature of the unfolding procedure. Indeed, consider that the effect of the response function is to smear a sharp peak into a wider distribution. The inverse problem thence has a tendency to take wide peaks and transform them into narrow peaks. Statistical fluctuations produce small peaks, which the inversion transforms into large peaks! The inverse problem is intrinsically unstable and thus seems doomed to failure.

Fortunately, instabilities can be tamed provided one is willing to introduce somewhat of a bias in the inversion procedure. This is a general feature of all estimators. The introduction of external constraints may reduce the variance of an estimator but results in a biased estimator. The result may nonetheless be acceptable if the bias is kept under control and reasonably small.

12.3.3 To Fold or Unfold, That Is the Question!

Unfolding of instrumental effects is challenging and prone to many numerical instabilities, as is painfully obvious from the discussion in the previous section. However, unfolding of instrumental effects is not always required. It may be sufficient to compare "raw" experimental data (i.e., not unfolded) with model calculations that account for instrumental effects. It is in fact much simpler to run model predictions through an experimental filter than to unfold experimental data. All that is needed is a sufficiently detailed model of the experimental response. In nuclear and particle physics, this is best accomplished with the GEANT package and a performance simulator specific to the apparatus. The idea is to simulate collisions and the production of particles according to the model of interest. The GEANT package is used to simulate the propagation of produced particles through the apparatus. It is possible to account for particle interactions within the detector, decays, and other forms of backgrounds as well as a detailed response of the apparatus. It is even possible to simulate varying or faulty performance of the instruments according to a

https://doi.org/10.1017/9781108241922.015 Published online by Cambridge University Press

detailed history of the performance of the apparatus. Model data filtered according to such a detailed simulation of the detector performance can then be meaningfully compared to experimental data. It is therefore possible to establish whether the model properly account for the observed data.

Comparisons of filtered theoretical models to experimental data are relatively common and quite useful in challenging the predictions of such theoretical models. The problem, however, is that in the absence of unfolded data, all theoretical models need to be propagated through the same experimental filter which accounts for all specificities and idiosyncrasies of the experiment. While it is in principle possible to publish a detailed description of the filter or even a computer code that replicates the filter, it is not always possible, in practice, because the filter may be too complex, or too fastidious to replicate and use. The complexity of the problem is further exacerbated if the experimental setup, particularly the trigger, is evolving through time. It must then be made clear which dataset and results correspond to which filter. It is also the case that the burden of proof, so to speak, is transferred to all scientists proposing a new model of the experimental data. It makes the comparison between models far less transparent and more prone to misrepresentations. How indeed can theorists be sure they are using the right experimental filter? This seems hardly fair. As a result, scientists tend to think that it is far more appropriate for experimenters to correct, that is, unfold their data for instrumental effects. It is also the case that the filtering of model predictions can grossly suppress features of interest and intuitive or explicit judgment of the validity of a model can be severely compromised.

Finally, and perhaps most importantly, detectors typically feature drastically different acceptance, resolution, and overall responses. Their effect on a measured observable may then be quite different. Any comparisons of uncorrected observables are consequently not possible or meaningful. Most scientists thus tend to regard the use of experimental filters to treat theoretical model predictions for comparison with experimental data as a last resort to be used exclusively when unfolding is too difficult or fraught with too many uncertainties.

12.3.4 Bin-by-Bin Method

The bin-by-bin method is commonly used in particle and nuclear physics to correct measurements of cross section and various other observables. The method is based on the assumption that bin-to-bin sharing is modest or negligible and that one can obtain a reasonable correction of measured data using a single multiplicative correction factor for each bin as follows:

$$\mu_i = C_i \left(n_i - \beta_i\right), \tag{12.48}$$

where β_i are background estimates for bin $i = 1, \ldots, m$, and C_i are coefficients designed to effect an appropriate correction of the measured distribution n_i to obtain a corrected distribution μ_i.

The coefficients C_i can generally be determined from MC simulations according to

$$C_i = \frac{\mu_i^{\mathrm{MC}}}{\nu_i^{\mathrm{MC}}}, \tag{12.49}$$

https://doi.org/10.1017/9781108241922.015 Published online by Cambridge University Press

where μ_i^{MC} represents the true signal generated by the MC model and ν_i^{MC} is the simulated experimental spectrum accounting for all relevant instrumental effects. Given sufficient computing power and resources, the coefficients C_i can in principle be determined with arbitrarily small statistical errors. If computing resources are scarce and statistical errors large, the usual methods of error propagation may be used to determine statistical errors on the corrected spectrum μ_i. However, it should be noted that strong correlations exist, by construction, between μ_i^{MC} and ν_i^{MC}. Care must thus be exercised in the estimation of errors on the coefficients C_i. A sensible determination of the errors may be accomplished with the unified approach discussed in §6.2.2 (frequentist approach) or by calculation of a credible region (Bayesian approach) based on the posterior probability $p(\mu_i^{\mathrm{MC}}|\nu_i^{\mathrm{MC}})$ as discussed in §7.2.4.

The bin-by-bin method is obviously much simpler in application than the unfolding procedure outlined in §12.3.1. But is it precise enough or susceptible of skewing the corrected distribution μ_i? The answer to this question, of course, depends on the response function R defined in §12.3.1. If R is essentially diagonal, one can write

$$R_{ij} \approx \delta_{ij}\varepsilon_j. \tag{12.50}$$

In this context, the background subtracted signal is simply

$$\nu_i^{\mathrm{signal}} = n_i - \beta_i = \varepsilon_i \mu_i. \tag{12.51}$$

The coefficients C_i are consequently the multiplicative inverse of the efficiencies ε_i. The bin-by-bin method thus amounts to an efficiency correction only. But when R is nondiagonal, the factors $1/C_i$ may become arbitrarily large, even larger than unity. The estimator $\hat{\mu}_i$ defined by (12.48) may thus be arbitrarily biased. Indeed, the expectation value of $\hat{\mu}_i$ is given by

$$\mathrm{E}\left[\hat{\mu}_i\right] = C_i \mathrm{E}\left[n_i - \beta_i\right] = C_i\left(\nu_i - \beta_i\right). \tag{12.52}$$

Inserting the values given by Eq. (12.49) for C_i, one finds

$$\mathrm{E}\left[\hat{\mu}_i\right] = \frac{\mu_i^{\mathrm{MC}}}{\nu_i^{\mathrm{MC}}}\nu_i^{\mathrm{sig}} \tag{12.53}$$

$$= \left(\frac{\mu_i^{\mathrm{MC}}}{\nu_i^{\mathrm{MC}}} - \frac{\mu_i}{\nu_i^{\mathrm{sig}}}\right)\nu_i^{\mathrm{sig}} + \mu_i, \tag{12.54}$$

in which the first term represents the estimator's bias. The covariance matrix U_{ij} of the corrected signals is evaluated in a similar fashion (see Problem 12.5).

$$U_{ij} = \mathrm{Cov}\left[\hat{\mu}_i, \hat{\mu}_j\right] = C_i^2 \mathrm{Cov}\left[n_i, n_j\right], \tag{12.55}$$

$$= C_i^2 \nu_i^{\mathrm{sig}} \delta_{ij}, \tag{12.56}$$

where, in the second line, we assumed the measured n_i are uncorrelated and determined by Poisson statistics.

The bias term B_i may be written

$$B_i = \left(\frac{1}{\varepsilon_i^{\mathrm{MC}}} - \frac{1}{\varepsilon_i^{\mathrm{true}}}\right)\nu_i^{\mathrm{sig}}. \tag{12.57}$$

https://doi.org/10.1017/9781108241922.015 Published online by Cambridge University Press

It is null only if the detection efficiencies determined by MC simulation, $\varepsilon_i^{\mathrm{MC}}$, are identically equal to the true (unknown) efficiency, $\varepsilon_i^{\mathrm{true}}$. However, this may be strictly possible only if the model properly reproduces the data perfectly and the simulation accounts for all instrumental effects appropriately. Since the MC model used to simulate the data is unlikely, in general, to perfectly reproduce the true signal, the estimator is by construction biased, and the bin-by-bin correction method shall lead to finite systematic errors. To the extent that the simulation provides a proper account of experimental effects, though, it is possible to use the bin-by-bin method iteratively to improve the correction coefficients. First, an arbitrary MC model is used to generate a first-order correction of the measured data. Then the corrected spectrum is used to produce a new set of MC data and evaluate tuned correction factors C_i', which can be used to produce a new updated corrected spectrum. The convergence of this iterative method can be tested with a **closure test** (see §12.4.7).

12.3.5 Correcting for Finite Bin Widths

Experimental distributions μ_i corrected for efficiency are commonly obtained with histograms of finite bin widths and must consequently be also be corrected for averaging effects through the bins. Recall from §12.3.1 that the values μ_i correspond to integrals (12.21) of the true distribution $f_t(x)$:

$$\mu_j = \mu_{\mathrm{tot}} \times p_j = \mu_{\mathrm{tot}} \int_{\mathrm{bin}\ j} dx_t f_t(x_t).$$

The value of the function $f_t(x)$ may thus be simply evaluated in each bin j as

$$f_t(x_j) = \frac{\mu_j}{\Delta x_j \mu_{\mathrm{tot}}}, \tag{12.58}$$

where $\Delta x_j = x_{\mathrm{max},j} - x_{\mathrm{min},j}$ corresponds to the width of bin j. It might be tempting to report this function by plotting the values $f_t(x_j)$ for each bin center position, $x_c = (x_{\mathrm{max},j} + x_{\mathrm{min},j})/2$. This would constitute a formally valid plot only if the function $f_t(x_j)$ varies linearly through all bins, however. Indeed, remember from our discussion in §4.6 that one can write

$$\int_{x_{\mathrm{min},i}}^{x_{\mathrm{max},i}} f(x)\,dx = f(x_i)\,(x_{\mathrm{max},i} - x_{\mathrm{min},i}) = f(x_{o,i})\Delta x_i,$$

where $x_{o,i}$ is a value of x within the interval $[x_{\mathrm{min},i}, x_{\mathrm{max},i}]$ but not the center of the bin in general. It is straightforward to show that the value $x_{o,i}$ corresponds to the center of the bin i only if the function $f(x_i)$ varies linearly though the bin. If $f(x)$ is nonlinear, one must use the dependence of the function in the vicinity of the bin i to estimate the appropriate value $x_{o,i}$. This can be accomplished by fitting a suitable model function $f_m(x; \vec{a})$ to the spectrum to obtain a parameterization $\vec{a}$ that enables calculation of the preceding integral for

https://doi.org/10.1017/9781108241922.015 Published online by Cambridge University Press

each bin:

$$I_i = \int_{x_{\min,i}}^{x_{\max,i}} f_m(x;\vec{a})\,dx = f_m(x_{o,i})\Delta x_i.$$

The values $x_{o,i}$ are then obtained by inversion of the function f_m, as follows:

$$x_{o,i} = f_m^{-1}(I_i/\Delta x_i). \tag{12.59}$$

As an example of application of this method, consider the determination of transverse momentum values $p_{T,i}$ that should be used to properly represent a transverse momentum spectrum $\frac{1}{p_T}\frac{dN}{dp_T}$. Since transverse momentum spectra measured in high-energy collisions are typically steeply falling, one can use a power law function

$$f_m(p_T) = A\left(1+\frac{p_T}{B}\right)^{-n} \tag{12.60}$$

to fit a spectrum $\frac{1}{p_T}\frac{dN}{dp_T}$. One writes

$$\frac{dN}{dp_T} = p_T f(_m(p_T) \tag{12.61}$$

$$I_i = \int_{\text{bin}-\text{i}} \frac{dN}{dp_T}dp_T = f(p_{T,i})\Delta p_i \tag{12.62}$$

$$= \int_{\text{bin}-\text{i}} p_T f_m(p_T)\,dp_T = \langle p_T\rangle_i \int_{\text{bin}-\text{i}} f_m(p_T)\,dp_T \tag{12.63}$$

where $\langle p_T\rangle_i$ is the mean p_T in bin i. Once the fit parameters A and B are known, one can thus get the values $p_{T,i}$ according to

$$p_{T,i} = \frac{\int_{\text{bin}-\text{i}} p_T f(p_T)\,dp_T}{\int_{\text{bin},i} f(p_T)\,dp_T}. \tag{12.64}$$

12.3.6 Unfolding with Regularization Methods

As we argued in §12.3.3, it is usually deemed preferable to correct raw data for instrumental effects rather than apply experimental filters on theoretical predictions to test theoretical models, and it is essential for proper comparison of results from different experiments. Since the bin-by-bin method is applicable only when the response matrix R_{ij} is diagonal or near diagonal, one is compelled to tackle the unfolding problem directly. Alas, a simple inversion of the response matrix typically leads to disastrous results: inverted spectra are numerically unstable and tend to feature wild oscillatory structures.

Meaningful unfolding is nonetheless possible. The general idea is to introduce a small bias in order to suppress fluctuations in the inverted instrumental response. This is accomplished by artificially imposing a smoothness constraint on the inverted solution using a smoothness function, $S(\vec{\mu})$, called the **regularization function**. The concept of regularization is rather general and is applied to machine learning and inverse problems. It involves the addition of possibly ad hoc information in order to solve an ill-posed problem or to

https://doi.org/10.1017/9781108241922.015 Published online by Cambridge University Press

prevent overfitting. It can be viewed in a Bayesian approach as imposing prior conditions on model parameters.

The use of a regularization function implies the obtained solution $\vec{\mu}$ will have a sub-optimal χ^2:

$$\chi^2 = \chi^2_{\text{min}} + \Delta\chi^2, \tag{12.65}$$

or likelihood:

$$\log L(\vec{\mu}) \sim \log L_{\text{max}} - \Delta \log L. \tag{12.66}$$

The key is to decide what deviation from the optimum, $\Delta\chi^2$ or $\Delta \log L$, can be meaningfully tolerated.

A wide range of regularization techniques and unfolding methods are documented in the scientific literature and commonly used in data analyses [13, 23, 48, 68, 91, 106]. A discussion of all these methods is well beyond the scope of this text. We focus our discussion on the singular value decomposition (SVD) method in §12.3.7 and the Bayesian unfolding method §12.3.8.

12.3.7 SVD Unfolding Method

We begin this section with a short summary of the notion of singular value decomposition in §12.3.7. An implementation of regularization in the context of the SVD method is presented in §§12.3.7 and 12.3.7. An example of application is presented in §12.3.7.

SVD of a Matrix

The SVD of a real $m \times n$ matrix $\mathbf{A}$ amounts to a factorization of the form

$$\mathbf{A} = \mathbf{U}\mathbf{S}\mathbf{V}^T, \tag{12.67}$$

where $\mathbf{U}$ and $\mathbf{V}$ are orthogonal matrices of size $m \times m$ and $n \times n$, respectively, while $\mathbf{S}$ is an $m \times n$ diagonal matrix with nonnegative diagonal elements. These conditions are expressed as follows

$$\mathbf{U}\mathbf{U}^T = \mathbf{U}^T\mathbf{U} = \mathbf{I}, \tag{12.68}$$

$$\mathbf{V}\mathbf{V}^T = \mathbf{V}^T\mathbf{V} = \mathbf{I}, \tag{12.69}$$

$$\mathbf{S}_{ij} = 0 \text{ for } i \neq j, \tag{12.70}$$

$$\mathbf{S}_{ii} = s_i \geq 0, \tag{12.71}$$

where the s_i are called **singular values** of the matrix $\mathbf{A}$, while the columns of $\mathbf{U}$ and $\mathbf{V}$ are known as the **left** and **right singular vectors**. One can verify that if $\mathbf{A}$ is itself orthogonal, all its singular values are equal to unity (see Problem 12.6), whereas a degenerate matrix features at least one null singular value.

https://doi.org/10.1017/9781108241922.015 Published online by Cambridge University Press

As it happens, a singular value decomposition is very useful toward the solution of linear equation systems of the type encountered in the unfolding problem

$$\mathbf{A}\vec{x} = \vec{b}, \tag{12.72}$$

where $\vec{x}$ and $\vec{b}$ are $n \times 1$ and $m \times 1$ column vectors, respectively. With $m \geq n$, the folded distribution $\vec{b}$ has more bins than $\vec{x}$ and thus constitutes an over constrained system. Formally, the solution of Eq. (12.72) may be written

$$\vec{x} = \mathbf{A}^{-1}\vec{b} = \left(\mathbf{USV}^T\right)^{-1}\vec{b} = \mathbf{VS}^{-1}\mathbf{U}^T\vec{b}, \tag{12.73}$$

and is exact provided the matrix $\mathbf{A}$ and the measured vector $\vec{b}$ have no errors. In practice, one finds that finite errors imply that diagonal elements s_i may be small and very imprecise for values i exceeding some threshold k. Hocker and Kartvelishvili [106] have shown that these components of the decomposition lead to solutions with fast numerical oscillations which render the technique ineffective unless a proper regularization technique is applied. We outline, in the next section, the procedure they developed to apply such a regularization.

SVD with Regularization

The unfolding of the overdetermined linear equation system (12.72) may be viewed as a solution of the least-squares problem

$$\chi^2 = \sum_{i=1}^{m}\left(\sum_{j=1}^{n} A_{ij}x_j - b_i\right)^2, \tag{12.74}$$

and is appropriate if the equations are exact or if the errors in $\vec{b}$ are all equal. But this is usually not the case, and it is thus better to consider a weighted least-squares system of equations

$$\chi^2 = \sum_{i=1}^{m}\left(\frac{\sum_{j=1}^{n} A_{ij}x_j - b_i}{\Delta b_i}\right)^2, \tag{12.75}$$

where Δb_i represent errors on b_i. With the inclusion of errors Δb_i, all terms i contribute more or less equally. If the errors on b_i and b_j are correlated, one must introduce a covariance matrix $B_{ij} = \mathrm{Cov}[b_i, b_j]$, and the preceding equation may be written in matrix form as

$$\chi^2 = \left(\mathbf{A}\vec{x} - \vec{b}\right)^T \mathbf{B}^{-1}\left(\mathbf{A}\vec{x} - \vec{b}\right). \tag{12.76}$$

The matrix $\mathbf{A}$ represents the probability that events in a bin i might end up in bin j. Since it is usually generated on the basis of Monte Carlo simulations (see §14.2.3), one typically ends up with a situation where rare i bins are not strongly populated and the corresponding coefficients A_{ij} may be artificially large (and even equal to unity) and rather imprecise thereby contributing a source of numerical oscillations. Hocker and Kartvelishvili [106] showed this problem can be partially mitigated by scaling the values A_{ij} and x_j

https://doi.org/10.1017/9781108241922.015 Published online by Cambridge University Press

according to

$$A_{ij} \to A'_{ij} = \lambda_j A_{ij} \quad \text{for } i = 1, m, \tag{12.77}$$
$$x_j \to x'_j = x_j/\lambda_j,$$

since these scalings do not formally change Eq. (12.72), but may be chosen to produce a matrix $\mathbf{A}'$ where statistically strong terms are large and weaker terms are small. This is achieved by introducing $\omega_j = x_j/x_j^{\text{mc}}$ where x_j^{mc} are the MC yields used to generate the matrix $\mathbf{A}$. One then writes

$$\sum_{j=1}^{n} A'_{ij}\omega_j = b_i, \tag{12.78}$$

which must be solved for ω_j. At the end of the unfolding procedure, one shall simply multiply these by x_j^{mc} to obtain the desired solutions x_j.

$$x_j = \omega_j \times x_j^{\text{mc}} \quad \text{for } j = 1, \ldots, n. \tag{12.79}$$

Typically, experimentalists aim to use MC models that provide a reasonable representation of the data. The values ω_j are thus approximately close to unity and feature only small fluctuations, thus requiring fewer terms in the SVD decomposition. The use of the scaled A'_{ij} also permit the statistics to be better represented with large terms, where statistical accuracy is large, and smaller terms otherwise. One can then proceed to obtain a formal solution which includes both scaled A'_{ij} coefficients and errors on b_i.

In general, the covariance matrix $\mathbf{B}$ may not be diagonal. But given it should be symmetric and positive definite, its SVD may be written

$$\mathbf{B} = \mathbf{QRQ}^T, \tag{12.80}$$

where $\mathbf{R}$ is a strictly diagonal matrix with $R_{ii} = r_i^2 \neq 0$. Its inverse $\mathbf{B}^{-1}$

$$\mathbf{B}^{-1} = \mathbf{QR}^{-1}\mathbf{Q}^T \tag{12.81}$$

can then be substituted in (12.76) with scaled $\mathbf{A}'$ and $\vec{\omega}$:

$$\chi^2 = \left(\mathbf{A}'\vec{\omega} - \vec{b}\right)^T \mathbf{QR}^{-1}\mathbf{Q}^T \left(\mathbf{A}'\vec{\omega} - \vec{b}\right). \tag{12.82}$$

Introducing

$$\tilde{A}_{ij} = \frac{1}{r_i}\sum_m Q_{im}A'_{mj}, \tag{12.83}$$
$$\tilde{b}_i = \frac{1}{r_i}\sum_m Q_{im}b_m,$$

one can write

$$\chi^2 = \left(\tilde{\mathbf{A}}\vec{\omega} - \tilde{b}\right)^T \left(\tilde{\mathbf{A}}\vec{\omega} - \tilde{b}\right). \tag{12.84}$$

Minimization of this χ^2 yields

$$\sum_j \tilde{A}_{ij}\omega_j = \tilde{b}_i, \tag{12.85}$$

https://doi.org/10.1017/9781108241922.015 Published online by Cambridge University Press

where $\tilde{b}_i$ now has a covariance equal to the unit matrix $\mathbf{I}$ and all equations i have the same weight. The problem remains, unfortunately, that an exact solution of this system of equations still features a rapidly oscillating distribution. But, it is now in a form such that spurious oscillatory components can be suppressed by a judicious choice of regularization. This is achieved in practice by writing,

$$\left(\tilde{\mathbf{A}}\vec{\omega} - \tilde{b}\right)^T \left(\tilde{\mathbf{A}}\vec{\omega} - \tilde{b}\right) + \tau \left(\mathbf{C}\vec{\omega}\right)^T \left(\mathbf{C}\vec{\omega}\right) = \min . \tag{12.86}$$

The matrix $\mathbf{C}$ defines the a priori condition on the solution of the equations and enables the implementation of a suitable regularization controlled by the regularization parameter τ. Given the solution is expected to be "smooth," it is reasonable to seek to minimize the local curvature of the distribution. This may be written

$$\sum_i \left[(\omega_{i+1} - \omega_i) - (\omega_i - \omega_{i-1})\right]^2 . \tag{12.87}$$

One then writes $\mathbf{C}$ as

$$\mathbf{C} = \begin{pmatrix} -1 & 1 & 0 & 0 & \cdots & 0 \\ 1 & -2 & 1 & 0 & \cdots & 0 \\ 0 & 1 & -2 & 1 & \cdots & 0 \\ 0 & & \cdots & & & \\ 0 & & \cdots & 1 & -2 & 1 \\ 0 & & \cdots & 0 & 1 & -1 \end{pmatrix} . \tag{12.88}$$

Minimization of Eq. (12.86) then leads to overdetermined system of equations

$$\begin{bmatrix} \tilde{\mathbf{A}} \\ \sqrt{\tau}\mathbf{C} \end{bmatrix} \omega = \begin{bmatrix} \tilde{b} \\ 0 \end{bmatrix} , \tag{12.89}$$

which can be solved by SVD. To avoid solving iteratively for several values of τ, Hocker and Kartvelishvili [106] found Eq. (12.89) may be written

$$\begin{bmatrix} \tilde{\mathbf{A}}\mathbf{C}^{-1} \\ \sqrt{\tau}\mathbf{I} \end{bmatrix} \mathbf{C}\omega = \begin{bmatrix} \tilde{b} \\ 0 \end{bmatrix} , \tag{12.90}$$

and solved for $\tau = 0$ provided one modifies the matrix $\mathbf{C}$ such that its inverse exists. One also needs to assume that the value s_i can be sorted in a nonincreasing sequence by appropriately swapping pairs of singular values. This can be accomplished by adding a small value ξ of order 10^{-3} or 10^{-4} to all terms of the diagonal:

$$\mathbf{C} = \begin{pmatrix} -1+\xi & 1 & 0 & 0 & \cdots & 0 \\ 1 & -2+\xi & 1 & 0 & \cdots & 0 \\ 0 & 1 & -2+\xi & 1 & \cdots & 0 \\ 0 & & \cdots & & & \\ 0 & & \cdots & 1 & -2+\xi & 1 \\ 0 & & \cdots & 0 & 1 & -1+\xi \end{pmatrix} . \tag{12.91}$$

For $\tau = 0$, a decomposition of $\tilde{\mathbf{A}}\mathbf{C}^{-1}$ may be expressed as

$$\tilde{\mathbf{A}}\mathbf{C}^{-1} = \mathbf{U}\mathbf{S}\mathbf{V}^T . \tag{12.92}$$

https://doi.org/10.1017/9781108241922.015 Published online by Cambridge University Press

Writing $\vec{d} = \mathbf{U}^T \tilde{b}$ and $\vec{z} = \mathbf{V}^T \mathbf{C}\vec{\omega}$, one then has

$$s_i \times z_i = d_i, \quad \text{for } i = 1, \ldots, n. \tag{12.93}$$

The orthogonality of $\mathbf{U}$ and the fact that the covariance matrix of $\tilde{b}$ is equal to unity insure that $\vec{d}$ also has unit covariance. Solution of (12.93) yields (for $\tau = 0$):

$$\begin{aligned} z_i^{(0)} &= \frac{d_i}{s_i}, \\ \vec{\omega}^{(0)} &= \mathbf{C}^{-1}\mathbf{V}\vec{z}^{\,(0)}. \end{aligned} \tag{12.94}$$

With $\tau = 0$, there is no regularization, so this solution is effectively useless. However, introducing finite (i.e., nonzero) values of τ, one can show that values d_i may be obtained according to

$$d_i^{(\tau)} = d_i \frac{s_i^2}{s_i^2 + \tau}, \tag{12.95}$$

which finally yield the sought for solution

$$\begin{aligned} z_i^{(\tau)} &= \frac{d_i s_i}{s_i^2 + \tau}, \\ \vec{\omega}^{(\tau)} &= \mathbf{C}^{-1}\mathbf{V}\vec{z}^{\,(\tau)}. \end{aligned} \tag{12.96}$$

A finite value of τ thus avoids numerical instabilities by effectively providing a cutoff of high-frequency terms (fast oscillations) of the decomposition.

The covariance matrices $\mathbf{Z}$ and $\mathbf{W}$ are found to be

$$\mathbf{Z}_{ik}^{(\tau)} = \frac{s_i^2}{\left(s_i^2 + \tau\right)^2}\delta_{ik}, \tag{12.97}$$

$$\mathbf{W}^{(\tau)} = \mathbf{W}^{-1}\mathbf{V}\mathbf{Z}^{(\tau)}\mathbf{C}^{-1}, \tag{12.98}$$

and the solution of the inverse problem thus become

$$x_i^{(\tau)} = x_i^{\text{mc}}\omega_i^{(\tau)}, \tag{12.99}$$

$$X_{ik}^{(\tau)} = x_i^{\text{mc}}\mathbf{W}_{ik}^{(\tau)}x_k^{\text{mc}}. \tag{12.100}$$

Choice of the Regularization Parameter τ and Errors

Plotting the values d_i (or $\ln|d_i|$) vs. i, one finds, typically, that the coefficients decrease with increasing i, until a value $i = k$ beyond which they oscillate or remain more or less constant because they are not statistically well determined. The critical value $i = k$ beyond which the coefficients d_i amount to Gaussian noise, can thus be used to set the regularization parameter

$$\tau = s_k^2. \tag{12.101}$$

The coefficients $s_i^2/(s_i^2 + \tau)$ in (12.95) suppress contributions $i > k$, and one obtains solutions with only modest fluctuations.

https://doi.org/10.1017/9781108241922.015 Published online by Cambridge University Press

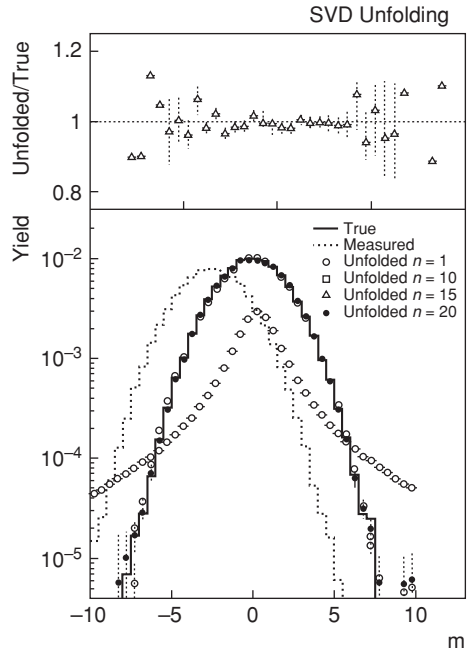

Fig. 12.5 Example of application of the SVD unfolding method. (Bottom panel) Simulated true (Gaussian) and measured distributions obtained with Gaussian smearing as described in the text; open and closed symbols represent unfolded distributions obtained after 1, 10, 15, and 20 applications of the SVD unfolding procedures. (Top panel) Ratio of the unfolded distribution obtained with 15 iterations to the true distribution. (Figure courtesy of S. Prasad.)

An alternative and effective technique to determine the optimal regularization parameter τ consists in generating a test spectrum $\vec{x}^{\text{test}}$ close but statistically distinct from the spectrum $\vec{x}^{\text{mc}}$ used to generate the unfolding matrix $\mathbf{A}$. One can then apply the folding and unfolding procedure onto $\vec{x}^{\text{mc}}$ and determine which value of τ yields a minimum χ^2, that is, such that the difference between the original test spectrum and its unfolded value best agree.

Hocker and Kartvelishvili [106] provide a detailed algorithm of the procedure as well as detailed examples. Functions to calculate SVD are available in a variety of software packages, including ROOT [59] with the class TDecompSVD.

Example of SVD Unfolding

We present an example of SVD unfolding accomplished with the RooUnfold framework [13] for a measurement of particle multiplicity. The generation of the response matrix R_{ij} is discussed in §14.2.3. We assume, arbitrarily, that the parent distribution has a Breit–Wigner shape with a mean of $\mu_t = 0.3$ and a width $\Gamma = 2.5$, while the response is described with a Gaussian distribution with a mean -2.5 and a standard deviation of 0.2. The true multiplicity distribution $P(m_t)$, shown with a solid line in Figure 12.5, is based on 100,000 events sampled from a Gaussian distribution centered at $m_t = 0$ and a standard

https://doi.org/10.1017/9781108241922.015 Published online by Cambridge University Press

deviation of 2.0. It was sampled and smeared with the preceding response function to generate the measured distribution, represented in Figure 12.5 with a dotted curve.

The SVD algorithm was used iteratively on the measured distribution, with the simulated response curve, to obtain the unfolded distributions shown in Figure 12.5 with open and closed points. One finds that a simple application of the unfolding method yields a distribution centered at the proper multiplicity but with a shape heavily reminiscent of the Breit-Wigner distribution used in the generation of the response matrix. However, the unfolded distribution obtained with 15 iterations of the procedure reproduces the true distribution extremely well and yields a ratio of the unfolded to true distribution which is within statistical errors, consistent with unity (top panel of the figure). In fact, a detailed study shows that the method yields numerically stable results, with unfolded to true distribution ratio equal to unity, within statistical errors, from 10 to 20 iterations. The SVD method is thus producing unfolding distributions that are robust and rather insensitive to the number of iterations, once convergence is achieved.

12.3.8 Bayesian Unfolding

As discussed in details in Chapter 7, **Bayesian inference** encompasses a wide range of techniques to learn about physical quantities (or scientific hypotheses) based on experimental data. Formally, it first requires the construction of deterministic and probabilistic models of the observable of interest and its dependencies on measurements and other assumed knowledge. In essence, this entails the determination of the probability of an event A might follow from an event B, noted $P(A|B)$, and the converse $P(B|A)$. In the context of an unfolding problem, B might represent the true spectrum whereas A would correspond to the measured data. The task is then to use a model of the measurement $P(A|B)$ based on some prior hypothesis for B, and rely on Bayes' theorem to inverse the problem and use the measured A to determine the true B. The technique is known as **Bayesian unfolding**, of which we present a brief outline largely following the seminal work of G. D'Agostini [73].

Inference models may be represented graphically as networks, called **Bayesian networks**, or **belief networks** [73]. Figure 12.6 illustrates a fit model used to establish the value of a parameter θ, which determines the relation between a dependent variable y and an independent variable x. The network explicitly identifies the components of the problem, their relations, and the assumptions used in the solution. The unfolding problem requires a slightly more elaborate network we introduce in the next section.

Bayesian Network

A Bayesian network can be regarded as a set of connections between nodes representing causes and effects. In the context of the unfolding problem, the causes correspond to the true values μ_i sought for, whereas the effects are the measured values n_i determined by the measurement protocol, the performance of the instruments (uncertainties and errors), and the actual values of the observables. A simple cause-and-effect network, sufficient for the description of the unfolding problem, is illustrated in Figure 12.7. The n nodes C_i represent the causes μ_i to be determined by unfolding whereas the m nodes E_j are effect

https://doi.org/10.1017/9781108241922.015 Published online by Cambridge University Press

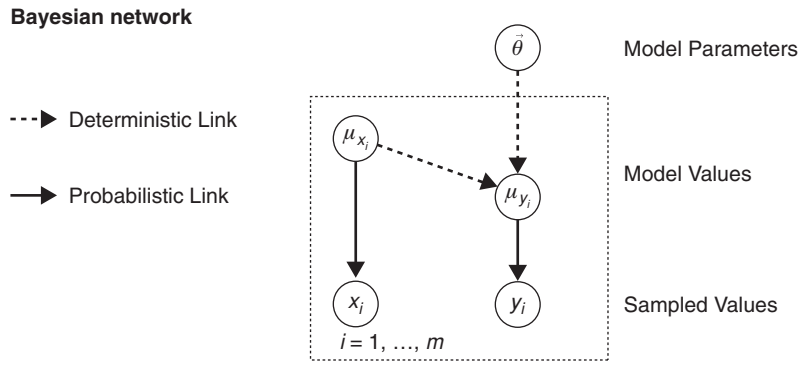

Fig. 12.6 Belief network used for the formulation of a model and fit of an experimental data distribution. The model parameters $\vec{\theta}$ are believed to lead to dependent values μ_{y_i} given independent values μ_{x_i} but the stochastic nature of the measurement process yields sampled values x_i and y_i for the independent and dependent values, respectively. One could enrich the network by including explicit assumptions concerning correlations between the variables and/or the width and bias of the fluctuations. (Adapted with permission from G. D'Agostini. Fits, and especially linear fits, with errors on both axes, extra variance of the data points and other complications. *ArXiv Physics e-prints*, November 2005.)

nodes, corresponding to measured n_j. The trash node T is used to represent detection inefficiencies: a certain fraction of each cause node C_i may remain undetected and ends up in the trash node.

The goal of unfolding is to find values $\vec{\mu} = (\mu_1(C_1), \ldots, \mu_n(C_n))$, given a set of measured effects $\vec{n} = (n_1(E_1), \ldots, n_m(E_m))$. The cause-to-effect links illustrated in Figure 12.7 have a probabilistic nature. Each cause C_i has a probability $P(E_j|C_i)$ of leading to an effect E_j. The inverse problem is thus statistical and probabilistic in nature also. Effectively, one must evaluate the probability $P(\vec{\mu}|\vec{n}, R, I)$ of the causes to be given by specific values $\vec{\mu}$ based on measured values $\vec{n}$, a response function R, and possibly some other system information I. As in previous sections of this chapter, the quantities n_j represent the number of

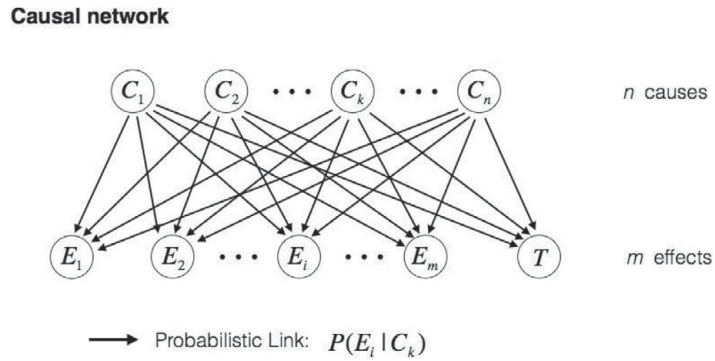

Fig. 12.7 Cause–effect network. The probabilistic links indicate the probability $P(E_i|C_k)$ a cause C_k may lead to an effect E_i. T is a trash node corresponding to "unmeasured events." (Adapted with permission from G. D'Agostini. Improved iterative Bayesian unfolding. *ArXiv e-prints*, October 2010.)

https://doi.org/10.1017/9781108241922.015 Published online by Cambridge University Press

"events" measured in bin j of the observable of interest x_m, while μ_i stands for the number of events of type C_i. By construction, R expresses the probability of observing a certain effect E_j given a specific cause C_i:

$$R_{ji} \equiv P(E_j|C_i, I) \tag{12.102}$$

where I once again represents what is known about the system (measurement protocol, instrument, etc.). The conditional probabilities are usually determined from MC simulations and consequently subjected to finite statistical uncertainties of their own. Given the probabilistic nature of the measurement process, the unfolding process is equally probabilistic, not deterministic. One can thus argue that the unfolding problem is a priori not amenable to a deterministic operation such as a matrix inversion, which also fails, as we saw, for purely technical reasons. This implies the need for a probabilistic solution of the problem instead of a simple matrix inversion, which effectively corresponds to a deterministic "rotation" in a space of n-dimensions.

One finds that the inversion "works" in the large number of events limit, such that stochastic effects are negligible and the observations $\vec{n}$ correspond to their expectation values ν. Indeed, the expectation values of n_j given the cause C_i can be written

$$\mathrm{E}\left[n_j|\mu_i\right] = P(E_j|C_i, I)\mu_i = R_{ji}\mu_i. \tag{12.103}$$

The expectation value of n_j given a set of causes $\vec{\mu}$ is thus

$$\mathrm{E}\left[n_j|\vec{\mu}\right] = \sum_{i=1}^{n} R_{ji}\mu_i, \tag{12.104}$$

or in matrix notation

$$\vec{n} = R\vec{\mu}, \tag{12.105}$$

which yields the known inverse problem

$$\mathrm{E}\left[\vec{\mu}\right] = R^{-1}\mathrm{E}\left[\vec{n}\right]. \tag{12.106}$$

where we explicitly include expectation values to emphasize that this result holds exclusively in the large number limit, that is, for the expectation values of $\vec{n}$, and not necessarily for a specific instance or measurement. Bayesian purists argue that the idea of inverting R is logically flawed because it is strictly valid for the expectation value of the measurements $\vec{n}$ not the actual measurements. However, as we saw, if the background is well known, then the preceding expression does yield, at least in principle, an unbiased estimator of $\vec{\mu}$.

Practical Considerations

By virtue of Bayes' theorem (Eq. 2.17) and the law of total probability (Eq. 2.19), one can write

$$P(\vec{\mu}|\vec{n}, R, I) = \frac{P(\vec{n}|\vec{\mu}, R, I)P(\vec{\mu}|I)}{\sum_{\vec{\mu}'} P(\vec{n}|\vec{\mu}', R, I)P(\vec{\mu}'|I)}, \tag{12.107}$$

https://doi.org/10.1017/9781108241922.015 Published online by Cambridge University Press

where the sum, in the denominator, is taken over all possible sets of events $\vec{\mu}'$ and essentially amounts to a normalization factor. The interesting components of the theorem reside in its numerator. The probability $P(\vec{n}|\vec{\mu}, R, I)$ is known as the likelihood of $\vec{n}$ given $\vec{\mu}$, the experimental response, and any other prior information I available about the system. It expresses the probability of obtaining a specific set of yields $\vec{n}$ given a set of values $\vec{\mu}$. The probabilities $P(\vec{\mu}|I)$ and $P(\vec{\mu}|\vec{n}, R, I)$ are known as **prior**, and **posterior**, respectively (For a detailed discussion of these concepts, see §§7.2.2 and 7.2.3). The prior expresses the probability of values $\vec{\mu}$ before a measurement is conducted (or perhaps based on prior measurements), while the posterior gives the probability of the values $\vec{\mu}$ after a measurement of $\vec{n}$ has been completed. Effectively, the preceding expression provides updated knowledge of the probability of a certain set of values $\vec{\mu}$ given a measurement $\vec{n}$. It is important to note that, nominally, the law of total probability does not yield a specific value $\vec{\mu}$ but rather the probability (or density of probability) of a specific set of values $\vec{\mu}$.

Clearly, the presence of a prior is logically required to obtain a posterior from the probability inversion provided by the law of total probability. But what prior should one use, since the choice should affect the outcome of the inversion? An obvious positive aspect of the notion of prior is that it enables one to insert in the solution of the inverse problem any knowledge that might be available ab initio about the system before the measurement is even attempted. That said, prior information is typically rather vague and may have a negligible impact on the inference process which then ends up being dominated by the likelihood $P(\vec{n}|\vec{\mu}, R, I)$. As we saw in §7.3, vagueness can be expressed by writing

$$P(\vec{\mu}|I) = \text{constant}. \tag{12.108}$$

The inference may then be performed according to the likelihood only:

$$P(\vec{\mu}|\vec{n}, R, I) \propto P(\vec{n}|\vec{\mu}, R, I). \tag{12.109}$$

The most probable spectrum $\vec{\mu}$ is thus the one that maximizes the likelihood in the absence of any contradictory information. The Bayesian approach effectively recovers the maximum likelihood estimators of the frequentist approach discussed in prior sections.

Given a full knowledge of the response function R, one could examine all values of $\vec{\mu}$, find their respective probabilities, obtain the most probable (or the expectation value), and consequently assess the uncertainty of the result. This is, however, not possible in practice with the usual knowledge one has of the likelihood function $P(\vec{n}|\vec{\mu}, R, I)$. To see why this is the case, consider the distribution of the cause events in bin C_i into all effect bins E_j. This can be described by a multinomial distribution

$$P(\vec{n}|\mu_i, R, I) = \frac{\mu_i!}{\prod_{k=1}^{m+1} n_k!} \prod_{j=1}^{m+1} {R_{ji}}^{n_j}. \tag{12.110}$$

The probability $P(\vec{n}|\vec{\mu}, R, I)$ is thus a sum of multinomial distributions – for which no closed formula exists.

https://doi.org/10.1017/9781108241922.015 Published online by Cambridge University Press

The elements of R are typically obtained by MC simulations. A large number of "events" is to be generated for each bin μ_i and one must count where they end up in n_j bins. Intuitively, one can write

$$R_{ji} = \frac{n_j^{\mathrm{MC}}}{\mu_j^{\mathrm{MC}}}. \tag{12.111}$$

One should, however, be aware of the fact that finite statistics in the generation of MC events leads to statistical errors on the coefficients. Bayes' theorem may be applied toward the determination of the coefficients R_{ji}. Defining column vectors R_i as $\vec{R}_i = (R_{1i}, R_{1i}, \ldots, R_{n+1,i})$, one can write

$$P(R_i|\vec{n}^{\,\mathrm{MC}}, \mu_i, I) \propto P(\vec{n}^{\,\mathrm{MC}}|\mu_i, R_i, I) \times P(R_i|I), \tag{12.112}$$

which provides a technique to improve our knowledge of the coefficient R_{ji}. Since $P(\vec{n}|\mu_i, R, I)$ is a multinomial distribution, it is convenient to choose a prior distribution in the form of a Dirichlet distribution (defined in §3.8):

$$P(\vec{\mu}^{\,\mathrm{prior}}|I) \propto p_1^{\alpha_1-1} p_2^{\alpha_2-1} \cdots p_m^{\alpha_m-1}, \tag{12.113}$$

where the values p_i express the probabilities of each cause i and the values α_i are specific values of the actual yield in each cause bin i. The multinomial and Dirichlet distributions are conjugate distributions (as defined in §7.3.3). Indeed, the product of a multinomial distribution by a Dirichlet distribution is itself a Dirichlet distribution with new values α_i'. It is thus possible to recalculate the coefficients based on these new values α_i'. This may also come in handy when estimating errors on the coefficients.

Basic Algorithm for Bayesian Unfolding

Bayes' theorem can be applied to the cause-and-effects bins to infer the (unknown) value of the cause bins. However, instead of using Eq. (12.107), one writes

$$P(C_i|E_i, I) = \frac{P(E_j|C_i, I) \times P(C_i|I)}{\sum_{k=1}^{m} P(E_j|C_k, I) \times P(C_k|I)}. \tag{12.114}$$

The probabilities $P(E_j|C_i, I) = R_{ij}$ are the likelihood, given by Eq. (12.102), of causes C_i yielding events in effect bins E_j, while the probabilities $P(C_i|I)$ represent the prior knowledge of the probability of the cause bins C_i. The probabilities $P(C_i|E_i, I)$ thus represent the posteriors or updated knowledge about the probability of the cause bins C_i. It is convenient to define coefficients θ_{ij} according to

$$\theta_{ij} = P(C_i|E_i, I) = \frac{R_{ji} P(C_i|I)}{\sum_{k=1}^{m} R_{jk} P(C_k|I)}. \tag{12.115}$$

In this formulation, the coefficients $P(C_i|I)$ assign a specific (prior) probability to the cause bins C_i, not the whole set of cause bins $\vec{\mu}$. If no prior information is available, one can set all bins to be equally probable. Note that this is different from assuming that all spectra $\vec{\mu}$

https://doi.org/10.1017/9781108241922.015 Published online by Cambridge University Press

are equally probable. Indeed, assuming a flat spectrum is far more restrictive than assuming that all spectra are equally probable. In practice, many implementations of the algorithm use the measured spectrum as the prior.

Given the probabilities θ_{ij}, one can share the counts (yields) of the measured bin E_j and estimate the causes according to

$$\mu_i|_{n_j} = P(C_i|E_j, I)n_j = \theta_{ij}n_j. \tag{12.116}$$

Summing over all observations, we get

$$\mu_i|_{\vec{n}} = \sum_{j=1}^{N} \theta_{ij}n_j. \tag{12.117}$$

We must also correct for efficiencies

$$\mu_i|_{\vec{n}} = \frac{1}{\varepsilon_i} \sum_{j=1}^{N} \theta_{ij}n_j, \tag{12.118}$$

where by definition

$$\varepsilon_i = \sum_{j=1}^{N} P(E_j|C_i, I) = \sum_{j=1}^{N} R_{ji} = 1 - R_{N+1,i}, \tag{12.119}$$

with coefficients R_{ij} estimated from MC studies with an appropriate simulation of the measurement according to

$$R_{ji} \approx \frac{n_j^{\mathrm{MC}}}{\mu_i^{\mathrm{MC}}}. \tag{12.120}$$

As already mentioned in the previous section, the accuracy of the coefficients R_{ij} is intrinsically limited by the statistical accuracy achieved in the determination of the yields n_j^{MC} and μ_i^{MC}. Since these two yields are correlated a priori by the MC generation process, it is prudent to avoid using the usual error propagation technique and instead make use of a sampling method.

By construction, the unfolded spectrum tends to "remember" the prior spectrum, and thus, it is convenient to iterate the preceding algorithm. Regularization and smoothing may also be added to the algorithm.

Bayesian Unfolding Example

Figure 12.8 displays an example of the application of Bayesian unfolding obtained with the response matrix, Figure 14.8, already used in §12.3.7 to illustrate SVD unfolding. Unfolded distributions are shown with open and closed symbols for 1, 3, 4, and 5 iterations of the algorithm. The top panel presents ratios of the unfolded distributions to the true distribution (solid line). One observes that the Bayesian method yields an unfolded distribution in excellent agreement with the true distribution, within statistical errors, and which is stable when repeated iteratively several times.

https://doi.org/10.1017/9781108241922.015 Published online by Cambridge University Press

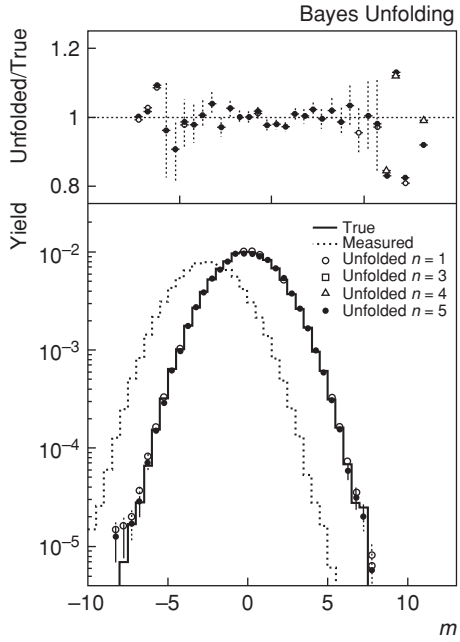

Fig. 12.8 Example of application of the Bayes unfolding method. (Bottom panel) Simulated true (Gaussian) and measured distributions obtained with Gaussian smearing as described in the text; open and closed symbols represent unfolded distributions obtained after 1, 3, 4, and 5 applications of the Bayesian unfolding procedures. Top panel: ratio of the unfolded to true distributions obtained with 4 and 5 iterations. (Figure courtesy of S. Prasad.)

12.4 Correcting Measurements of Correlation Functions

Integral and differential correlation functions are defined in terms of combinations of single-, two-particle, and more generally multiparticle yields (or cross sections). As such they are subjected to the same instrumental limitations and distortions as the yields on which they are based. The impact of instrumental effects may be exacerbated by the fact that the determination of cumulants involves subtraction of two or more terms of similar magnitude. So while instrumental effects on cross sections (or production yields) may be relatively modest, they can have disastrous consequences on correlation functions, most particularly when correlations are weak because of dilution effects associated with large numbers of correlation sources. Fortunately, correlation functions expressed in terms of ratios of cumulants to products of single-particle yields are approximately robust, that is, independent of detection efficiencies. They thus lend themselves to a variety of simple correction techniques that are relatively easy to implement.

We begin with a discussion of issues involved in the correction of measurement of variance, which leads us naturally into a discussion of the robustness of ratios of factorial moments and corrections of differential correlation functions. Irreducible instrumental

https://doi.org/10.1017/9781108241922.015 Published online by Cambridge University Press

effects associated with variations in the instrumental response are discussed in the latter part of this section.

12.4.1 Correction Of Integrated Yield Measurements

Measurements of integrated particle production yields over a finite kinematic range are of interest as estimators of collision hardness (e.g., in proton–proton interactions) or collision centrality (e.g., in heavy-ion collisions) and for measurements of yield fluctuations. Insofar as the kinematic volume of integration considered is much larger than the resolution of the kinematical parameters of interest, smearing effects may be neglected and one is chiefly concerned with correcting for detector efficiencies.

From a theoretical standpoint, the average integrated yield, $\langle N \rangle$, over a specific kinematic domain, Ω, is determined by the particle production cross section (see §10.2):

$$\langle N \rangle = \int_{\Omega} \frac{d^3N}{dp^3} dp^3. \tag{12.121}$$

Experimentally, however, one observes that the produced number of particles fluctuates collision by collision owing to the stochastic nature of the particle production process. The fluctuations may be described by a probability function, $P_{\text{prod}}(N)$, determined by the dynamics and correlations involved in the particle production process. The average multiplicity is thus

$$\langle N \rangle = \int_0^{\infty} P_{\text{prod}}(N) N dN. \tag{12.122}$$

Measurements of particle production are usually subject to losses and a variety of other instrumental effects. For large detectors, one can usually assume that the probability of detecting one particle is independent of the probability of detecting others. One can then model the detection of a single-particle with a Bernoulli distribution (defined in §3.1). Let ε represent the probability to measure any produced particle in the kinematic domain Ω:

$$\begin{aligned} P_{\text{single}}(n|\varepsilon) &= 1 - \varepsilon \quad \text{probability of not observing,} \;\; n = 0 \\ &= \varepsilon \qquad \text{probability of observing,} \;\; n = 1. \end{aligned} \tag{12.123}$$

As we saw in §3.1, the probability of obtaining n successes out of N trials determined by the same Bernoulli distribution amounts to a binomial distribution. We can then express the probability of simultaneously detecting n particles in the domain Ω as a binomial distribution with success probability ε:

$$P_{\text{det}}(n|N, \varepsilon) = \frac{N!}{n!(N-n)!} \varepsilon^N (1-\varepsilon)^{N-n}. \tag{12.124}$$

For fixed N, the distribution has a mean (see Table 3.1)

$$\langle n \rangle_{\text{N}} = \text{E}[n] = \int P_{\text{det}}(n|N, \varepsilon) n \, dn = \varepsilon N, \tag{12.125}$$

https://doi.org/10.1017/9781108241922.015 Published online by Cambridge University Press

and a variance

$$\langle (n - \langle n \rangle)^2 \rangle_{\mathrm{N}} = \int P_{\mathrm{det}}(n|N, \varepsilon)\,(n - \langle n \rangle)^2\, dn \tag{12.126}$$
$$= N\varepsilon(1 - \varepsilon).$$

One must account, however, for fluctuations of N according to $P_{\mathrm{prod}}(N)$. The probability of observing n particles may then be written

$$P_{\mathrm{meas}}(n|\varepsilon) = \int dN P_{\mathrm{det}}(n|N, \varepsilon) P_{\mathrm{prod}}(N). \tag{12.127}$$

The mean measured multiplicity $\langle n \rangle$ can be calculated in terms of $\langle N \rangle$ even if $P_{\mathrm{prod}}(N)$ is unknown:

$$\langle n \rangle = \int dn n P_{\mathrm{meas}}(n|\varepsilon), \tag{12.128}$$
$$= \int dn n \int dN P_{\mathrm{det}}(n|N, \varepsilon) P_{\mathrm{prod}}(N). \tag{12.129}$$

Indeed, changing the order of integration, we get

$$\langle n \rangle = \int dN P_{\mathrm{prod}}(N) \int dn n P_{\mathrm{det}}(n|N, \varepsilon), \tag{12.130}$$
$$= \varepsilon \int dN P_{\mathrm{prod}}(N) N, \tag{12.131}$$
$$= \varepsilon \langle N \rangle. \tag{12.132}$$

We thus formally obtain the intuitively obvious result that one can correct the measured average multiplicity by simply dividing by the efficiency of the measurement:

$$\langle N \rangle = \frac{\langle n \rangle}{\varepsilon}. \tag{12.133}$$

This result is correct even in cases where the efficiency varies over time. To demonstrate this, let us assume, for simplicity's sake, that an experiment can be divided into two time periods featuring particle detection efficiencies ε_1 and ε_2. Let us also assume that the probability of observing the events during the two time periods is unmodified by this change, and let us denote the number of events detected in the two periods as N_1^{ev} and N_2^{ev}.

The average multiplicities measured during the two periods are noted $\langle n_i \rangle$ with $i = 1,\ 2$. Given the definition of efficiency and the preceding result, one can write

$$\langle n_i \rangle = \varepsilon_i \langle N \rangle. \tag{12.134}$$

The average efficiency is calculated as a weighted average of the efficiencies of the two periods

$$\varepsilon_{\mathrm{avg}} = \frac{N_1^{\mathrm{ev}} \varepsilon_1 + N_2^{\mathrm{ev}} \varepsilon_2}{N_1^{\mathrm{ev}} + N_2^{\mathrm{ev}}}. \tag{12.135}$$

The multiplicity measured across the two periods is:

$$\langle n \rangle = \varepsilon_{\mathrm{avg}} \langle N \rangle. \tag{12.136}$$

https://doi.org/10.1017/9781108241922.015 Published online by Cambridge University Press

Extraction of the true mean multiplicity $\langle N \rangle$ can thus be obtained for either time periods

$$\langle N \rangle = \frac{\langle n \rangle_1}{\varepsilon_1} = \frac{\langle n \rangle_2}{\varepsilon_2}, \tag{12.137}$$

or globally from the average of the two periods,

$$\langle N \rangle = \frac{\langle n \rangle}{\varepsilon_{\text{avg}}}, \tag{12.138}$$

since

$$\langle n \rangle_{\text{avg}} = \frac{N_1^{\text{ev}} \langle n \rangle_1 + N_2^{\text{ev}} \langle n \rangle_2}{N_1^{\text{ev}} + N_2^{\text{ev}}} \tag{12.139}$$

$$= \frac{N_1^{\text{ev}} \varepsilon_1 \langle N \rangle + N_2^{\text{ev}} \varepsilon_2 \langle N \rangle}{N_1^{\text{ev}} + N_2^{\text{ev}}} \tag{12.140}$$

$$= \frac{N_1^{\text{ev}} \varepsilon_1 + N_2^{\text{ev}} \varepsilon_2}{N_1^{\text{ev}} + N_2^{\text{ev}}} \langle N \rangle \tag{12.141}$$

$$= \varepsilon_{\text{avg}} \langle N \rangle. \tag{12.142}$$

This conclusion can clearly be generalized to multiple time periods when the detection efficiency might have taken different values. For measurements of average particle production yields, it thus does not matter that the experimental response changes over time as long as one can track these changes and estimate the detection efficiency during each period independently or globally for the entire data-taking run. This means that insofar as it possible to obtain an average efficiency, it is not necessary to carry the analysis of each time period separately; and one can use Eq. (12.138) to determine the average produced particle yield. However, we will see in the next section that such simple treatment is not warranted for measurements of fluctuations and correlation functions.

The detection efficiency is rarely uniform across the acceptance of a measurement. One must thus also consider whether the average efficiency correction procedure outlined earlier is robust when the detection efficiency is a function of kinematical variables. For simplicity's sake, let us partition the measurement acceptance into two parts of size Ω_1 and Ω_2 with respective efficiencies ε_1 and ε_2. The average multiplicity measured in these two regions may be written

$$\langle n_i \rangle = \varepsilon_i \langle N_i \rangle, \tag{12.143}$$

where

$$\langle N_i \rangle = \int_{\Omega_i} \frac{d^3N}{dp^3} dp^3, \tag{12.144}$$

with the full kinematical range Ω corresponding to

$$\Omega = \sum_{i=1}^{2} \Omega_i. \tag{12.145}$$

https://doi.org/10.1017/9781108241922.015 Published online by Cambridge University Press

The average number of produced particles can be properly determined by summing corrected yields in parts 1 and 2 individually:

$$\langle N\rangle = \sum_{i=1}^{2}\langle N_i\rangle = \sum_{i=1}^{2}\frac{\langle n_i\rangle}{\varepsilon_i}. \tag{12.146}$$

If the fractions $f_i = \langle N_i\rangle/\langle N\rangle$ of the total yield produced in the two parts of the acceptance are known a priori, one can write an average efficiency (as in the case of the time-varying efficiency discussed earlier):

$$\varepsilon_{\text{avg}} = \frac{f_1\varepsilon_1 + f_2\varepsilon_2}{f_1 + f_2} = f_1\varepsilon_1 + f_2\varepsilon_2, \tag{12.147}$$

since $f_1 + f_2 = 1$ by definition. Unfortunately, the fractions f_i are in general not known a priori, and it is thus not possible to formally define a model independent average efficiency across the full acceptance Ω. However, in cases where the production cross section is nearly constant within the experimental acceptance, one can write

$$f_i = \frac{\int_{\Omega_i}\frac{d^3N}{dp^3}dp^3}{\int_{\Omega}\frac{d^3N}{dp^3}dp^3} \approx \frac{\int_{\Omega_i}dp^3}{\int_{\Omega}dp^3} = \frac{\Omega_i}{\Omega}, \tag{12.148}$$

which satisfies $\sum_i f_i = 1$. The size of the fractions f_i is then fixed by the relative sizes of the Ω_i, and a model independent average efficiency can be formulated. The efficiency correction, defined by Eq. (12.138), is thus applicable in spite of the fact the efficiency may vary through the acceptance of the measurement.

12.4.2 The Unfriendly Variance

Studies of the variance (as well as higher moments) of physical observables are often of interest to probe the dynamics of physical systems. We have discussed in §11.3.3, for instance, that the study of fluctuations of the net charge of produced particles or ratios of species integrated yields are particularly useful to probe the collision dynamics of large nuclei at relativistic energies. Unfortunately, while the variance of an observable is in principle a good measure of its fluctuations, correcting a measurement of variance for instrumental effects is anything but trivial. For illustrative purposes, let us continue the discussion initiated in the previous section and examine how the detection efficiency affects the variance of the measured integrated yield within a specific acceptance Ω.

We use Eq. (12.127) to calculate the variance of the measured multiplicity:

$$\text{Var}[n] = \langle(n - \langle n\rangle)^2\rangle = \langle n^2\rangle - \langle n\rangle^2. \tag{12.149}$$

The mean $\langle n\rangle$ is known from Eq. (12.130). The calculation of the second moment $\langle n^2\rangle$ proceeds as in (12.130):

$$\begin{aligned}\langle n^2\rangle &= \int dNP_{\text{prod}}(N)\int dn n^2 P_{\text{det}}(n|N,\varepsilon),\\ &= \int dNP_{\text{prod}}(N)N\varepsilon(1-\varepsilon+N\varepsilon),\\ &= \varepsilon(1-\varepsilon)\langle N\rangle + \varepsilon^2\langle N^2\rangle,\end{aligned} \tag{12.150}$$

https://doi.org/10.1017/9781108241922.015 Published online by Cambridge University Press

where in the second line we used the second moment of the binomial distribution (see Table 3.1) and in the third line the definition of the average $\langle N \rangle$ and $\langle N^2 \rangle$. The variance of the measured distribution is thus

$$\mathrm{Var}[n] = \varepsilon^2 \mathrm{Var}[N] + \varepsilon(1-\varepsilon)\langle N \rangle. \tag{12.151}$$

This expression contains terms linear and quadratic in ε. Correcting the measured variance of the multiplicity thus cannot be achieved by dividing the measured variance by the square of the efficiency as one might intuitively be inclined to do. Since one is usually interested in detecting small deviations of the variance from values expected for a Poisson distribution, it is thus imperative that the efficiency ε be known very accurately. Unfortunately, achieving the required level of efficiency is often rather challenging, and it may not be possible to reliably correct the measured variance.

All is not lost, however, since two alternative approaches are possible. The first approach involves a measurement of factorial moments while the second is based on a comparison of the measured variance with that obtained with mixed events (defined in §12.4.5). Both approaches are commonly used in practical applications.

The variance of integrated particle yields is determined by the production dynamics of the particle and the extent to which the produced particles are correlated. It can thus be regarded as having a purely "statistical" or Poisson component, σ^2_{stat}, and a "dynamical" component, $\Delta\sigma^2_{\mathrm{dyn}}$. Instrumental effects may unfortunately modify the size of the variance and introduce a "shift" $\Delta\sigma^2_{\mathrm{inst}}$. The measured variance may thus be written

$$\sigma^2_{\mathrm{meas}} = \sigma^2_{\mathrm{stat}} + \Delta\sigma^2_{\mathrm{dyn}} + \Delta\sigma^2_{\mathrm{inst}}. \tag{12.152}$$

The Poisson component is trivial and of limited interest. Measurements thus typically aim at the identification of the dynamical component. Unfortunately, this component is often much smaller than the size of the correction implied by Eq. (12.151). A precise assessment of the efficiency correction is therefore essential to achieve a meaningful measurement.

Rather than attempting a precise evaluation of the efficiency and other instrumental effects based on some simulation model of an experiment, it is possible to use the data itself to estimate the efficiency based on the mixed-event technique. As its name suggests, this technique, consists in synthesizing artificial events based on actual data by mixing particles from different actual events. Particles produced in different events are de facto noncorrelated by the production process but bear the effects of the instrumentation. The variance or correlation function of mixed events should thus be determined solely by the stochastic nature of the production process and instrumental effects. Since particles from different events are uncorrelated, the variance of integrated yields should be determined by Poisson statistics as well as correlation induced by detector effects. Under ideal conditions (discussed later in this chapter) one can hypothesize that the instrumental effects are essentially identical for real and mixed events. One can thus write

$$\sigma^2_{\mathrm{mixed}} = \sigma^2_{\mathrm{stat}} + \Delta\sigma^2_{\mathrm{inst}}. \tag{12.153}$$

https://doi.org/10.1017/9781108241922.015 Published online by Cambridge University Press

Subtraction of the variance of mixed events from that of real events therefore enables, in principle, the extraction of the dynamical component of the variance:

$$\Delta\sigma^2_{\text{dyn}} = \sigma^2_{\text{meas}} - \sigma^2_{\text{mixed}}. \tag{12.154}$$

It is important to realize that the dynamical correlations may either increase or decrease the variance of the integrated yield. The dynamical component $\Delta\sigma^2_{\text{dyn}}$ may be positive or negative, respectively. For negative values of $\Delta\sigma^2_{\text{dyn}}$, it is obviously not meaningful to extract a square root and quantify dynamical effects as an imaginary value. The fact of the matter is that the value $\Delta\sigma_{\text{dyn}}$, that is, without the square, is not particularly significant. This shift is really the result of correlation effects involving two or more particles. It can indeed be positive, negative, or even null. The temptation to extract a square root is thus simply an artifact of the poor historical choice of notation used to denote dynamical fluctuations.

Correcting for detector effects and the determination of the dynamical correlation may also be carried out based on ratios of factorial moments and corrected measurements of integrated multiplicity. The variance of the measured integrated yield, $\langle(n - \langle n\rangle)^2\rangle$, may be written

$$\langle(n - \langle n\rangle)^2\rangle = \langle n^2\rangle - \langle n\rangle^2. \tag{12.155}$$

Inserting $-\langle n\rangle + \langle n\rangle$ yields

$$\langle(n - \langle n\rangle)^2\rangle = \langle n^2\rangle - \langle n\rangle + \langle n\rangle - \langle n\rangle^2, \tag{12.156}$$

$$= \langle n(n-1)\rangle + \langle n\rangle - \langle n\rangle^2. \tag{12.157}$$

We thus find that the variance of n may be expressed in terms of the factorial moment $\langle n(n-1)\rangle$ and two terms that depend on the mean multiplicity $\langle n\rangle$. Recall from §10.2 that the difference $\langle n(n-1)\rangle - \langle n\rangle^2$ corresponds to a factorial cumulant C_2, which constitutes a proper measure of particle correlations. One can thus write

$$\langle(n - \langle n\rangle)^2\rangle = C_2 + \langle n\rangle. \tag{12.158}$$

Since the intent of a measurement of variance is to identify the strength of particle correlations, the preceding expression suggests that rather than measuring the variance of n, one should measure the cumulant C_2 directly. We will see in the next section that while the cumulant C_2 is itself dependent on the detection efficiency, the correlation function R_2 obtained by dividing C_2 by the square of the integrated average multiplicity is in fact independent of detection efficiencies and thus constitutes a robust observable. Measurements of C_2 or R_2 should thus be favored over measurements of variances insofar as the intent is to identify correlations induced by particle production dynamics.

12.4.3 Correcting Differential Correlation Functions and Factorial Cumulants

Robustness of Normalized Cumulants R_2

We demonstrated in §10.2 that cumulants and factorial cumulants constitute genuine measures of particle correlations, while n-particle densities suffer from trivial "combinatorial

https://doi.org/10.1017/9781108241922.015 Published online by Cambridge University Press

backgrounds" and thus do not provide a reliable measure of correlations. We will now proceed to show that ratio of differential cumulants and factorial cumulants to products of single-particle yields are robust variables. We begin our demonstration with two-particle correlation functions and show that the robust ratios can be trivially extended to higher order cumulants.

Measurements of single- and two-particle differential cross sections (e.g., $dN/d\eta$) are usually carried out using histograms with bins of finite width. Recall from §4.6 that one can estimate functions by dividing the histogram bin content (already scaled by the number of integrated events to obtain a per event average) by the width(s) of the bins:

$$\hat{f}(x_i) = \frac{h_i}{\Delta x_i}, \tag{12.159}$$

$$\hat{f}(x_i, y_j) = \frac{h_{i,j}}{\Delta x_i \Delta y_j}. \tag{12.160}$$

Estimates of the single-particle differential cross section, $\rho_1(x) \equiv dN/dx$, and two-particle differential cross section, $\rho_2(x_1, x_2) \equiv dN/dx_1 dx_2$ expressed as a function of some kinematical variable x (e.g., the transverse momentum, the pseudo-rapidity, etc.) may then be written

$$\hat{\rho}_1(x_i) = \frac{\langle N(x_i)\rangle}{\Delta x_i}, \tag{12.161}$$

$$\hat{\rho}_2(x_{1,i}, x_{2,j}) = \frac{\langle N(x_{1,i})N(x_{2,j})\rangle}{\Delta x_{1,i}\Delta x_{2,j}}, \tag{12.162}$$

where $\langle N(x_i)\rangle$ and $\langle N(x_i)N(x_j)\rangle$ are the average number of particles in bin i and the average number of pairs of particles in bins i and j, respectively.

$$\langle N(x_i)\rangle = \int_{\text{bin,i}} \frac{dN}{dx} dx, \tag{12.163}$$

$$\langle N(x_{1,i})N(x_{2,j})\rangle = \int_{\text{bin,i}} dx_1 \int_{\text{bin,j}} dx_2 \frac{d^2N}{dx_1 dx_2}. \tag{12.164}$$

Experimentally, instrumental losses may occur. Ignoring smearing effects, the measured average number of particles in bin i and pairs of particles in bins i and j are thus

$$\langle n(x_i)\rangle = \varepsilon_1(x_i)\langle N(x_i)\rangle, \tag{12.165}$$

$$\langle n(x_{1,i})n(x_{2,j})\rangle = \varepsilon_2(x_{1,i}, x_{2,j})\langle N(x_{1,i})N(x_{2,j})\rangle. \tag{12.166}$$

One can then define estimators of the observed single-particle density and two-particle densities as follows:

$$\hat{\nu}_1(x_i) = \langle n(x_i)\rangle/\Delta x_i, \tag{12.167}$$

$$\hat{\nu}_2(x_{1,i}, x_{2,j}) = \langle n(x_{1,i})n(x_{2,j})\rangle/\Delta x_i \Delta x_j. \tag{12.168}$$

Based on the preceding expressions, we can write

$$\hat{\nu}_1(x_i) = \varepsilon_1(x_i)\hat{\rho}(x_i), \tag{12.169}$$

$$\hat{\nu}_2(x_{1,i}, x_{2,j}) = \varepsilon_2(x_{1,i}, x_{2,j})\hat{\rho}_2(x_{1,i}, x_{2,j}), \tag{12.170}$$

https://doi.org/10.1017/9781108241922.015 Published online by Cambridge University Press

where $\varepsilon_1(x_i)$ is the efficiency for detecting particles in bin x_i and $\varepsilon_2(x_{1,i}, x_{2,j})$ is the joint efficiency corresponding to the probability of simultaneously observing particles in bins $x_{1,i}$ and $x_{2,j}$.

In general, for particles emitted at different momenta and directions, it is reasonable to assume that $\varepsilon_2(x_{1,i}, x_{2,j})$ may be expressed as a simple product of the single-particle efficiencies, that is the efficiencies for independently observing each particle in bins x_i and x_j:

$$\varepsilon_2(x_{1,i}, x_{2,j}) = \varepsilon_1(x_{1,i})\varepsilon_1(x_{2,j}). \tag{12.171}$$

One can then readily verify that the ratio r_2 and the correlation function R_2 defined in §11.1.1 by Eqs. (10.36) and (10.37) are robust variables. Indeed, calculating r_2 in terms of measured densities $\hat{\nu}_1(x_i)$ and $\hat{\nu}_2(x_{1,i}, x_{2,j})$, we have

$$\hat{r}_2^{\text{meas}}(x_{1,i}, x_{2,j}) = \frac{\hat{\nu}_2(x_{1,i}, x_{2,j})}{\hat{\nu}_1(x_{1,i})\hat{\nu}_1(x_{2,j})}. \tag{12.172}$$

Inserting the expressions (12.170) and (12.169) for $\hat{\nu}_2$ and $\hat{\nu}_1$, respectively, we get

$$\hat{r}_2^{\text{meas}}(x_{1,i}, x_{2,j}) = \frac{\varepsilon_1(x_{1,i})\varepsilon_1(x_{2,j})\hat{\rho}_2(x_{1,i}, x_{2,j})}{\varepsilon_1(x_{1,i})\hat{\rho}_1(x_{1,i})\varepsilon_1(x_{2,j})\hat{\rho}_1(x_{2,j})}, \tag{12.173}$$

$$= \frac{\hat{\rho}_2(x_{1,i}, x_{2,j})}{\hat{\rho}_1(x_{1,i})\hat{\rho}_1(x_{2,j})}, \tag{12.174}$$

$$= \hat{r}_2^{\text{prod}}, \tag{12.175}$$

which is the definition of the normalized cross section r_2 expressed in terms of the produced densities $\hat{\rho}_1(x_{1,i})$, $\hat{\rho}_1(x_{2,j})$, and $\hat{\rho}_2(x_{1,i}, x_{2,j})$. Since $R_2 = r_2 - 1$, we conclude that both r_2 and R_2 are independent of detection efficiency and thus robust observables.

However, note that whenever the bins x_i and x_j are identical, the number of pairs must be calculated as $\langle n(x_i)(n(x_i) - 1)\rangle$. The preceding formulas are otherwise unchanged. Our discussion also holds irrespective of the size of the bins used to carry out the analysis as long as smearing effects are negligible. We thus conclude that our statement of robustness holds for both differential and integral correlation functions (factorial cumulants).

Rather than measuring $R_2(x_1, x_2)$, it is often sufficient or more appropriate to consider the dependence of the cumulant on the difference $\Delta x = x_1 - x_2$ (e.g., $\Delta\varphi = \varphi_1 - \varphi_2$, or $\Delta\eta = \eta_1 - \eta_2$ and report $R_2(\Delta x)$. As we discussed in §11.1.2, this can be viewed as an average over the domain spanned by the variable $\bar{x} = (x_1 + x_2)/2$ determined by the acceptance for x_1 and x_2:

$$\hat{R}_2(\Delta x) = \frac{1}{\Omega(\Delta x)} \int_{\Omega(\Delta x)} d\bar{x} \hat{R}_2(\Delta x, \bar{x}). \tag{12.176}$$

Since $R_2(\Delta x, \bar{x})$ may be obtained directly from $R_2(x_1, x_2)$ by means of a change of variables $x_1, x_2 \to \Delta x, \bar{x}$, it is by construction also independent of detection efficiencies and consequently robust. However, recall from §11.1.1 that two distinct methods may be used

https://doi.org/10.1017/9781108241922.015 Published online by Cambridge University Press

to estimate the function $\hat{R}_2(\Delta x)$. Method 2 yields the preceding formula (12.176) and is consequently robust by construction, while Method 1 is based on a ratio of averages:

$$\hat{R}_2(\Delta x) = \frac{\hat{\nu}_2(\Delta x)}{\nu_1 \otimes \nu_1(\Delta x)}, \tag{12.177}$$

where the product $\nu_1 \otimes \nu_1(\Delta x)$ is typically determined based on a mixed-event method:

$$\nu_1 \otimes \nu_1(\Delta x) = \hat{\nu}_2^{\text{Mixed}}(\Delta x). \tag{12.178}$$

Formally, the density $\hat{\nu}_2(\Delta x)$ may be calculated as

$$\hat{\nu}_2(\Delta x) = \frac{1}{\Omega(\Delta x)} \int_{\Omega(\Delta x)} d\bar{x} \hat{\nu}_2(\Delta x, \bar{x}), \tag{12.179}$$

while the product $\nu_1 \otimes \nu_1(\Delta x)$ may be similarly written

$$\hat{\nu}_1 \otimes \nu_1(\Delta x) = \frac{1}{\Omega(\Delta x)} \int_{\Omega(\Delta x)} d\bar{x} \hat{\nu}_1(x_1) \hat{\nu}(x_2). \tag{12.180}$$

Substituting the expressions for $\hat{\nu}_2(\Delta x, \bar{x})$ and $\nu_1(x_i)$ in Eq. (12.177), we get

$$\hat{R}_2^{\text{meas}}(\Delta x) = \frac{\int_{\Omega(\Delta x)} d\bar{x} \varepsilon_1(x_{1,i}) \varepsilon_1(x_{2,j}) \hat{\rho}_2(x_1, x_2)}{\int_{\Omega(\Delta x)} d\bar{x} \varepsilon_1(x_{1,i}) \rho_1 \varepsilon_1(x_{2,j}) \rho_1(x_2)}. \tag{12.181}$$

Clearly, if the efficiencies $\varepsilon_1(x_1)$ and $\varepsilon_1(x_2)$ have explicit dependencies on x_1 or x_2, the preceding expression shall yield a ratio R_2 that may differ appreciably from the result obtained with Eq. (12.176). We thus conclude that Method 1 cannot be considered robust in general. However, if the efficiencies are constant throughout the acceptance of the measurement, than they can be factored out of the integral and hence cancel out of Eq. (12.181). Method 1 can thus be considered approximately robust. Noting that $\nu_2(\Delta x, \bar{x})$ may be written $\nu_1(x_1)\nu_1(x_2)R_2(\Delta x, \bar{x})$, the preceding expression can be rewritten as

$$\hat{R}_2^{\text{M1}}(\Delta x) = \frac{\int_{\Omega(\Delta x)} d\bar{x} \varepsilon_1(x_1) \rho_1 \varepsilon_1(x_2) \rho_1(x_2) R_2(\Delta x, \bar{x})}{\int_{\Omega(\Delta x)} d\bar{x} \varepsilon_1(x_1) \rho_1 \varepsilon_1(x_2) \rho_1(x_2)}. \tag{12.182}$$

We thus conclude that the ratio (12.181) shall also be robust if $\hat{R}_2(\Delta x, \bar{x})$ is approximately independent of $\bar{x}$:

$$\hat{R}_2^{\text{M1}}(\Delta x) \approx \hat{R}_2(\Delta x, \bar{x}) \frac{\int_{\Omega(\Delta x)} d\bar{x} \varepsilon_1(x_1) \rho_1 \varepsilon_1(x_2) \rho_1(x_2)}{\int_{\Omega(\Delta x)} d\bar{x} \varepsilon_1(x_1) \rho_1 \varepsilon_1(x_2) \rho_1(x_2)}, \tag{12.183}$$

$$= \hat{R}_2(\Delta x, \bar{x}). \tag{12.184}$$

So, although R_2 may depend on Δx, Method 1 shall remain robust as long as it is constant for any given value of Δx, in other words, $R_2(\Delta x, \bar{x}) = K(\Delta x)$, where $K(\Delta x)$ is some smooth function of Δx but independent of $\bar{x}$.

One can also show that Method 1 yields a robust result for azimuthal correlations (e.g., functions of $\Delta\varphi$) with periodic boundary conditions (see Problem 12.1).

https://doi.org/10.1017/9781108241922.015 Published online by Cambridge University Press

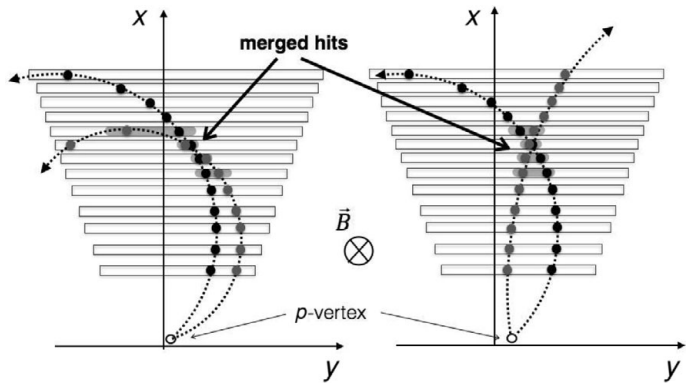

Fig. 12.9 Schematic illustration of track merging between equal sign and unequal sign charged particle tracks. The rectangular boxes indicate detection planes while dark circles represent the track energy deposition and detected hits. Wherever two tracks pass in close proximity the hits they produced may end up merging. The disturbed shape and centroid of these hits hinder the track reconstruction quality and efficiency.

Basic Instrumental Effects

Neither Method 1 nor Method 2 is robust for particle pairs featuring a small separation $\Delta\eta$, $\Delta\varphi$, and Δp_T. As illustrated in Figure 12.9, like-sign charged particles with similar momenta traverse the detector in close proximity of another and may thus not be well resolved. Such two tracks may then appear to partially or totally merge with one another. In the same way, unlike-sign particles with similar $\Delta\eta$ and $\Delta\varphi$ may cross the detection planes at nearly identical positions and become unresolved, thereby also resulting in track pair losses. **Track merging** and **track crossing** thus create an irreducible loss of particle pairs. Effectively, this implies the joint efficiency ε_2 does not factorize for particle pairs with $\Delta\eta \approx 0$, $\Delta\varphi \approx 0$, and $\Delta p_T \approx 0$. The observables r_2 and R_2 are consequently not robust for particles with small track separation.

In complex detectors consisting of multiple segments or components, it is also possible for tracks to become broken, as shown in Figure 12.10. There is typically a finite probability that a single track might be reconstructed as two or more tracks, resulting in a phenomenon known as **track splitting**. This produces extra tracks which artificially increase the average particle yield $\langle n \rangle$ and create artificial particle correlations. Splitting produces like-sign tracks with very similar parameters (e.g., η, φ, and p_T) and may thus produce artificially enhanced correlations for pairs with $\Delta\eta \approx 0$, $\Delta\varphi \approx 0$, and $\Delta p_T \approx 0$. In data analyses, particularly for measurements of correlation functions, effects associated with track splitting may be easily suppressed by using exclusively tracks that feature a number of hits well in excess of half of the number of possible hits.

The notion of robustness also breaks down when detectors are operated in occupancy conditions that exceed their design specifications. Detector occupancy refers to the fraction of detector sensors being "hit" at any given time. In low track or hit multiplicity environments, the probability of track or hit merging is small, and ambiguities resulting in track merging or splitting are typically limited. However, high-occupancy conditions may

https://doi.org/10.1017/9781108241922.015 Published online by Cambridge University Press

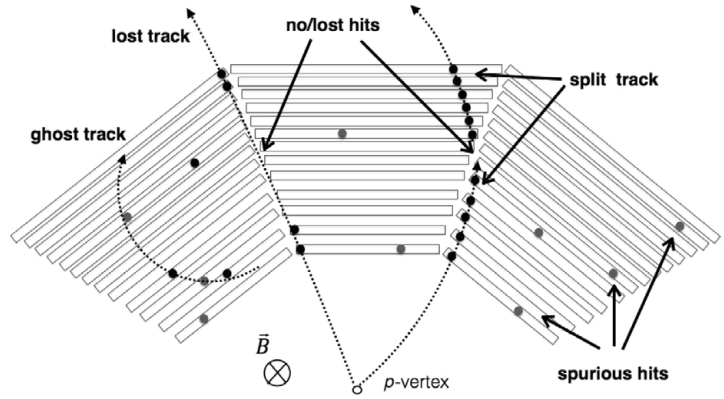

Fig. 12.10 Schematic illustration of split tracks, ghost tracks, as well as lost tracks.

induce ambiguities in hit and track reconstruction, as illustrated in Figure 12.10, which result in the reconstruction of false tracks, also known as **ghost tracks**. Admixtures of ghost tracks may impair the reconstruction efficiency of proper tracks and induce instrumental correlations if they are limited to specific regions of a complex detector. The reconstruction of uncorrelated ghost tracks may also change the magnitude of the normalized cumulant R_2 because the artificially inflated single-track density increases the size of its denominator but not its numerator. A similar effect may be produced by the decay of long-lived particles such as K_s^0 or Λ^0.

The robustness of correlation functions may be impaired by a variety of other instrumental effects, some of which we discuss in the next section.

Instrumentally Induced Correlations

We have seen in §12.4.3 that the normalized density r_2 and normalized cumulant R_2 are robust when measured according to Method 2 and to a lesser extent when estimated with Method 1, even when the efficiency varies throughout the acceptance of the measurement. However, the robustness is lost if the detection efficiency varies with time or event-by-event relative to some global event parameter. Let us illustrate this statement for a detection system featuring two performance states, that is, with efficiency of detection globally taking two distinct values for two classes of events, either separated in time, run, or some other "external" parameter.

For simplicity's sake, let us assume a correlation measurement between identical particles in the same kinematic range. The detection of both particles of the pair thus has the same efficiency dependence on the measured coordinates. However, let us also assume that two distinct classes of events of knowable size (i.e., how many events belong to each class) exist and feature different detection efficiencies we shall denote as ε_i, with $i = 1, 2$. The approach discussed here will hold for higher numbers of performance classes. We saw earlier in this chapter that is possible to define an effective or average efficiency ε_{avg}, provided the relative sizes of the two event classes are known. This average efficiency may then be

https://doi.org/10.1017/9781108241922.015 Published online by Cambridge University Press

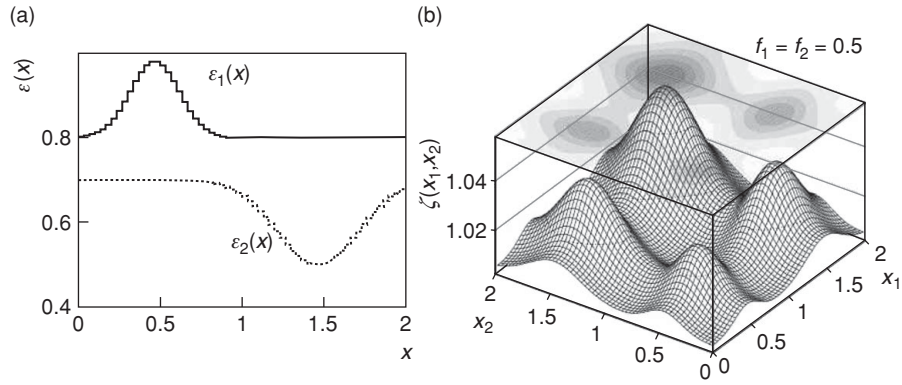

Fig. 12.11 (b) Robustness function $\xi(x_1, x_2)$ for a two-performance state experiment calculated for the efficiencies shown in (a), and assuming the same amount of data were acquired with the two efficiency curves.

used to correct average single-particle densities according to Eq. (12.133). Such correction is unfortunately not possible for correlation functions if the two sets of events are mixed. To demonstrate this statement, let us define the fraction of events reconstructed with efficiencies ε_i as f_i, and satisfying $\sum_i f_i = 1$. Let us also assume the two-particle efficiency factorizes (i.e., $\varepsilon_i(x_1, x_2) = \varepsilon_i(x_1)\varepsilon_i(x_2)$). If the data are analyzed indiscriminately of event classes, the measured single-particle and two-particle densities may be written

$$\hat{n}_1(x) = [f_1\varepsilon_1(x) + f_2\varepsilon_2(x)]\,\rho_1(x), \tag{12.185}$$

$$\hat{n}_2(x_1, x_2) = [f_1\varepsilon_1(x_1)\varepsilon_1(x_2) + f_2\varepsilon_2(x_1)\varepsilon_2(x_2)]\,\rho_2(x_1, x_2). \tag{12.186}$$

It is thus easy to verify that the ratio r_2 is not robust under such circumstances:

$$\hat{r}_2^{\text{meas}}(x_1, x_2) = \xi(x_1, x_2)\hat{r}_2(x_1, x_2),$$

with

$$\hat{r}_2(x_1, x_2) \equiv \frac{\rho_2(x_1, x_2)}{\rho_1(x_1)\rho_1(x_2)}, \tag{12.187}$$

and

$$\xi(x_1, x_2) = \frac{f_1\varepsilon_1(x_1)\varepsilon_1(x_2) + f_2\varepsilon_2(x_1)\varepsilon_2(x_2)}{[f_1\varepsilon_1(x_1) + f_2\varepsilon_2(x_1)]\,[f_1\varepsilon_1(x_2) + f_2\varepsilon_2(x_2)]}. \tag{12.188}$$

which is manifestly different from unity in general. The function $\xi(x_1, x_2)$ measures the extent to which the robustness of the observable r_2 is broken by having different efficiencies for two classes of events. This is illustrated in Figure 12.11, which displays the function $\xi(x_1, x_2)$ for two arbitrary efficiency curves $\varepsilon_1(x)$ and $\varepsilon_2(x)$ and $f_1 = f_2 = 0.5$ corresponding to a situation where an equal amount of data is acquired with the efficiency curves. All this said, it is quite remarkable that while large and arbitrary nonuniformities (of order 10–20%) have been assumed in the efficiency distributions shown in Figure 12.11, their "average" leads to relatively small deviations of less than 5%. This maximum difference

https://doi.org/10.1017/9781108241922.015 Published online by Cambridge University Press

essentially amounts to half the difference between the two spatial averages of the efficiencies. The R_2 observable thus remains relatively robust in spite of the time dependence of the efficiency. The necessity to correct for such effects is then determined by the level of accuracy sought after in the measurement, as well as the size of these variable efficiency features.

If the efficiencies $\varepsilon_i(x)$ are actually independent of x but depend on time, one finds that the factor $\xi(x_1, x_2)$ merely produces a shift in the amplitude of the correlation function. However, in cases where $\varepsilon_i(x)$ varies appreciably with x, particularly near the edges of the acceptance, variations of $\varepsilon_i(x)$ with external conditions or parameters such as the detector occupancy or the collision vertex position may induce sizable artificial structures throughout a correlation function [163]. Such effects may also be induced at the boundaries between detector components with performances that vary in time or with external conditions such as the detector occupancy.

Robustness of the r_2 and R_2 observables may be recovered, at least partially, if the analysis may be carried according to event classes, that is, by measuring these observables for each event class independently and combining the measurements into a global average.

$$r_2^{\text{class}}(x_1, x_2) = f_1 \frac{\varepsilon_1(x_1)\varepsilon_1(x_2)\rho_2(x_1, x_2)}{\varepsilon_1(x_1)\rho_1(x_1)\varepsilon_1(x_2)\rho_1(x_2)} + f_2 \frac{\varepsilon_2(x_1)\varepsilon_2(x_2)\rho_2(x_1, x_2)}{\varepsilon_2(x_1)\rho_1(x_1)\varepsilon_2(x_2)\rho_1(x_2)}. \quad (12.189)$$

The efficiencies cancel out and one gets

$$r_2^{\text{class}}(x_1, x_2) = f_1 \frac{\rho_2(x_1, x_2)}{\rho_1(x_1)\rho_1(x_2)} + f_2 \frac{\rho_2(x_1, x_2)}{\rho_1(x_1)\rho_1(x_2)}, \quad (12.190)$$

$$= r_2(x_1, x_2), \quad (12.191)$$

since, by definition, $f_1 + f_2 = 1$. This form of computation enables full-use of datasets even though the efficiency may vary with time or experimental conditions. The technique is applicable, in particular, for measurements of correlation functions where the acceptance and efficiency are dependent on the position of the collision vertex. It then suffices to bin the analysis of two- and single-particle densities in terms of the position of the vertex. With n bins, corrected yields and correlations may thus be obtained with

$$r_2^{\text{class}}(x_1, x_2) = \sum_{i=1}^{n} f_i \frac{\nu_{2,i}(x_1, x_2)}{\nu_{1,i}(x_1)\nu_{1,i}(x_2)}, \quad (12.192)$$

where the coefficients f_i represent the relative frequency of events in each z-vertex bin and satisfy $\sum_{i=1}^{n} f_i = 1$.

Collision Centrality Averaging in Heavy-Ion Collisions

In studies of high-energy heavy-ion collisions, it is useful and convenient to study the strength of single-particle yields and correlation functions as a function of collision centrality estimated on the basis of global event observables, such as the total transverse energy, zero degree energy, or integrated multiplicity measured in a selected portion of the detector acceptance. Two types of experimental effects must be accounted for in principle. The first effect arises because cumulants and single-particle yields scale differently with

https://doi.org/10.1017/9781108241922.015 Published online by Cambridge University Press

the number of sources of correlated particle production, while the second effect has to do with possible efficiency dependencies on the event multiplicity (i.e., number of particles produced in an event) or the detector occupancy.

First, consider that given sufficient statistics and computing resources, it should be possible to determine the normalized two-particle density r_2 as a function of some collision impact measure, b, with arbitrarily fine granularity (resolution) using Method 2:

$$r_2(x_1, x_2|b) = \frac{\rho_2(x_1, x_2|b)}{\rho_1(x_1|b)\rho_1(x_2|b)}. \tag{12.193}$$

An average can then be taken over collision centralities in a specific range $[b_{\min}, b_{\max}]$:

$$r_2(x_1, x_2|[b_{\min}, b_{\max}]) = \int_{b_{\min}}^{b_{\max}} r_2(x_1, x_2|b)P(b)\,db, \tag{12.194}$$

where $P(b)$ is a PDF expressing the probability of collisions of centrality b. In practice, it may not be possible to measure the single and pair densities with fine granularity. One then gets densities as averages over collision centrality between the limits, $b_{\min}$, and $b_{\max}$.

$$\rho_1(x|[b_{\min}, b_{\max}]) = \int_{b_{\min}}^{b_{\max}} \rho_1(x|b)P(b)\,db, \tag{12.195}$$

$$\rho_2(x_1, \eta_2|[b_{\min}, b_{\max}]) = \int_{b_{\min}}^{b_{\max}} \rho_2(x_1, x_2|b)P(b)\,db. \tag{12.196}$$

An estimate of the correlation function (Eq. 12.194) can then be obtained from the ratio of the averages.

$$r_{2,\text{est}}(x_1, x_2|[b_{\min}, b_{\max}]) = \frac{\rho_2(x_1, x_2|[b_{\min}, b_{\max}])}{\rho_1(x_1; [b_{\min}, b_{\max}])\rho_1(x_2|[b_{\min}, b_{\max}])} - 1. \tag{12.197}$$

This estimate is biased, however, by the finite centrality bin width used in the measurement. To demonstrate this bias, let us approximate the densities as

$$\rho_1(x_1|b) = n(b)h_1(x_1), \tag{12.198}$$

$$\rho_2(x_1, x_2|b) = n(b)(n(b) - 1)h_2(x_1, x_2), \tag{12.199}$$

where $n(b)$ and $n(b)(n(b) - 1)$ denote the average single and pair densities evaluated as function of the centrality parameter b, while the functions $h_1(x_1)$ and $h_2(x_1, x_2)$ denote the dependence of the number of singles and pairs on the position x_1 and x_2, and are here assumed, for simplicity's sake, to be independent of collision centrality. The preceding estimate of the correlation function then becomes

$$r_{2,\text{est}}(x_1, x_2|[b_{\min}, b_{\max}]) = Q(b_{\min}, b_{\max})\frac{h_2(x_1, x_2)}{h_1(x_1)h_1(x_2)}, \tag{12.200}$$

with

$$Q(b_{\min}, b_{\max}) = \frac{\int_{b_{\min}}^{b_{\max}} n(b)\,(n(b) - 1)\,P(b)\,db}{\left(\int_{b_{\min}}^{b_{\max}} n(b)P(b)\,db\right)^2}, \tag{12.201}$$

https://doi.org/10.1017/9781108241922.015 Published online by Cambridge University Press

which is clearly different than the result obtained with Eq. 12.194

$$\int_{b_{\min}}^{b_{\max}} \frac{n(b)\,(n(b)-1)}{n(b)n(b)} P(b)\,db, \tag{12.202}$$

which tends to unity in the large $n(b)$ limit. The estimate Eq. (12.200) is consequently more and more biased with increasing bin width. This effect may, however, be suppressed by dividing $R_{2,\text{est}}$ explicitly by $Q(b_{\min}, b_{\max})$. Such correction could not compensate, however, for possible dependencies of the shape of the functions $h_1(x_1)$ and $h_2(x_1, x_2)$ with the centrality parameter b. If the data sample is sufficiently large, the best approach is thus to carry the analysis in fine bins of b, which one can then subsequently combine, by weighted average, into wider centrality bins.

The estimate Eq. (12.200) is not only biased as a result of the width of the centrality bin but also intrinsically nonrobust against detection efficiencies. Indeed, since detection efficiencies typically decrease with higher detector occupancy, one expects particle tracks produced in high-multiplicity collisions (central collisions) to be reconstructed with smaller efficiencies than those produced in peripheral or low-multiplicity collisions. This dependence effectively produces different classes of events, each with a different efficiency response through the detector acceptance. Average of correlation function across finite centrality bins may thus be subjected to instrumentally induced changes in amplitude or shape. To illustrate this, let us express the efficiency as a function $\varepsilon(x|M)$ of collision centrality measured by some global observable M. The robustness measure $\xi(x_1, x_2)$ may then be written (see Problem 12.2)

$$\xi(x_1, x_2) = \frac{\int dM P(M)\varepsilon(x_1|M)\varepsilon(x_2|M)}{\int dM P(M)\varepsilon(x_1|M) \int dM' P(M')\varepsilon(x_2|M')}, \tag{12.203}$$

where $P(M)$ corresponds to the probability of events with centrality M, with $\int dM P(M) = 1$ within a specific centrality bin. It is quite obvious that unless $P(M)$ is constant across a bin, or the efficiency independent of M, the factor $\xi(x_1, x_2)$ shall in general deviate from unity and contribute a bias in the estimation of correlation functions. This issue can be avoided, in principle, if it is possible to use fine centrality bins and calculate the correlation function according to Eq. (12.192). This calculation technique yields properly corrected and robust correlation functions in the limit of very narrow centrality bins. Its feasibility may, however, be limited by the size of the data sample. If too fine a binning in b is attempted, the sampled single-particle yield $\rho_1(x|b)$ may be null in one or several x bins. The ratio $R_2(x_1, x_2|b)$ would then diverge in those x bins, and the method would consequently fail. This implies that, in practice, it is necessary to systematically test the correction method and verify its convergence while changing the impact parameter bin size used to carry out centrality bin-width corrections.

Weighing Techniques

We saw in §12.4.3 that whenever the detection efficiency exhibits dependencies on global event observables such as the vertex position, detector occupancy, or beam instantaneous luminosity, one may need to partition the data analysis into a large number of different

https://doi.org/10.1017/9781108241922.015 Published online by Cambridge University Press

bins in order to obtain conditions under which detection efficiencies are approximately constant within one bin. Correlation studies typically require large-size histograms and may thus consume a large amount of computer memory. Having to replicate the same histograms several times to account for efficiency dependencies may become a cumbersome and memory expensive proposition. Fortunately, a simple solution exists in the form of a weighing technique.

Weighing techniques are rather general and may be used toward the study of R_2 as well as other types of correlation functions such as $\langle \Delta p_{\mathrm{T}} \Delta p_{\mathrm{T}}(\Delta\eta, \Delta\phi)\rangle$ discussed in §11.1.5. The weights are designed to be inversely proportional to the detection efficiency and as such equalize the detector response. A technique to obtain them is discussed below. Once the weights are available, one can proceed to carry out the correlation analysis using either Method 1 or Method 2, and by incrementing histograms with weights $\omega(\eta_1, \phi_1, p_{\mathrm{T},1})\times \omega(\eta_2, \phi_2, p_{\mathrm{T},2})$ rather than unity, for R_2 analyses, and $\omega(\eta_1, \phi_1, p_{\mathrm{T},1}) \times \omega(\eta_2, \phi_2, p_{\mathrm{T},2}) \times \Delta p_{\mathrm{T},1} \times \Delta p_{\mathrm{T},2}$ for $\langle \Delta p_{\mathrm{T}} \Delta p_{\mathrm{T}}\rangle$ analyses.

In the context of correlation studies carried out as a function of $\Delta\eta$ vs. $\Delta\phi$, one must account for the fact that detection efficiencies are complicated functions of ϕ, η, and p_{T} that may evolve with the position, z, of the collision vertex. One must consequently obtain weights, $\omega(\eta, \phi, p_{\mathrm{T}}, z)$, that depend simultaneously on all four of these variables. The weights thus acquire a dual function: they account for the z dependence as well as the p_{T} versus ϕ dependencies simultaneously. The purpose of the weights is to equalize the response in p_{T} across all values of ϕ, η, and for all z. They can therefore be calculated as

$$\omega(\eta, \phi, p_{\mathrm{T}}, z) = \frac{\int d\phi \int d\eta \int_{z_{\min}}^{z_{\max}} dz \langle n(\eta, \phi, p_{\mathrm{T}}, z)\rangle}{\langle n(\eta, \phi, p_{\mathrm{T}}, z)\rangle}, \tag{12.204}$$

where the integration on ϕ and η covers the fiducial acceptance of interest. By construction, the p_{T} spectra and $\langle p_{\mathrm{T}}\rangle$ become independent of ϕ as well as η. Independence relative to η is likely acceptable at LHC and RHIC in the context of narrow η acceptance detectors such as STAR and ALICE, but better η dependent treatment may be required for wider acceptances.

Realistic detector performance simulations can be used to estimate absolute detection efficiencies as a function of track parameters as well as global event conditions (e.g., centrality, detector occupancy, etc.) and calculate weights, $\omega(\eta, \phi, p_{\mathrm{T}})$, in terms of their multiplicative inverse.

$$\omega(\eta, \phi, p_{\mathrm{T}}) = \frac{1}{\varepsilon(\eta, \phi, p_{\mathrm{T}})}. \tag{12.205}$$

Alternatively, detection efficiencies may also be estimated using embedding techniques (§12.4.6).

12.4.4 Flow Measurement Corrections

Measurements of flow correlation functions such as those defined in §11.4 require the determination of the flow plane angle Ψ and nominally assume this angle is uniformly

https://doi.org/10.1017/9781108241922.015 Published online by Cambridge University Press

distributed in the $[0, 2\pi[$ range. In practice, this is rarely the case because of various instrumental effects. Fortunately, there exist several simple techniques to remedy this problem.

The first technique, known as **Phi weighing**, gives each *particle* a weight $\omega(\phi)$ proportional to the inverse of the azimuthal distribution $h(\phi)$ of the particles averaged over a large ensemble of events.

$$\omega(\phi) = \left(\frac{h(\phi)}{\frac{1}{n_\phi} \sum_\phi h(\phi)} \right)^{-1}, \tag{12.206}$$

where n_ϕ is the number of bins in ϕ.

The second technique, called **recentering**, uses a modified event **Q**-vector obtained by subtracting an event averaged **Q**-vector from each event's nominal **Q**-vector.

$$\vec{Q}'_n = \vec{Q}_n - \langle \vec{Q}_n \rangle. \tag{12.207}$$

The third technique, commonly referred to as **shifting**, gives a weight $\omega(\Psi)$ to *events* based on the event ensemble distribution of reaction plane angles $h(\Psi)$.

$$\omega(\Psi) = \left(\frac{h(\Psi)}{\frac{1}{n_\Psi} \sum_\Psi h(\Psi)} \right)^{-1}, \tag{12.208}$$

where n_Ψ is the number of bins in Ψ.

Other correction techniques are also documented in the literature [182].

12.4.5 Mixed-Event Correction Technique

Event mixing is a technique commonly used to decorrelate observables that can be combined into one quantity, such as the invariance mass of particle pairs, two-, or multiparticle correlation functions. The technique was initially developed in the context of analyses of intensity interferometry of pions to obtain uncorrelated particle pairs and determine effects of acceptance and detection efficiency directly from data [131]. The method was extended later on for the generation of background distributions for a wide range and variety of correlation functions, invariant mass distributions, and many other applications.

Event mixing involves the generation of "artificial" events consisting of uncorrelated objects (hits, charged particle tracks, jets, etc.) based on actual data. Objects are sampled from different events and are as such physically uncorrelated, that is, from the point of view of production processes. Their detection is nonetheless subject to essentially all instrumentation effects (e.g., detector resolution, acceptance, efficiency, etc.). The analysis of mixed events enables correlation analyses of ab initio uncorrelated objects and thus provides a baseline for actual correlation measurements.

As a practical example, let us consider a measurement of the normalized cumulant $R_2(\varphi_1, \varphi_2)$ for particles produced in nucleus–nucleus collisions. Recall from §10.2.4 that

https://doi.org/10.1017/9781108241922.015 Published online by Cambridge University Press

R_2 is defined as a ratio of the cumulant $C_2(\varphi_1, \varphi_2)$ by the product of measured single particle densities $\nu_1(\varphi_1)\nu_1(\varphi_2)$:

$$R_2(\varphi_1, \varphi_2) = \frac{C_2(\varphi_1, \varphi_2)}{\nu_1(\varphi_1)\nu_1(\varphi_2)}, \tag{12.209}$$

$$= \frac{\nu_2(\varphi_1, \varphi_2)}{\nu_1(\varphi_1)\nu_1(\varphi_2)} - 1. \tag{12.210}$$

In a background-free measurement, the measured densities are determined by the production cross section and detection efficiencies. Rather than trying to determine the efficiencies explicitly, one can mobilize the fact that R_2 is by construction a robust observable and utilize mixed events to estimate the denominator of the correlation function. The basic idea of the event-mixing technique is to "fabricate" artificial events consisting of an equal number of particles (tracks) as actual events, but with tracks selected randomly from a large pool of events of similar characteristics. One can then proceed to analyze these mixed events as if they were real events and obtain mixed two-particle densities $\nu_2^{\text{mix}}(\varphi_1, \varphi_2)$. Since the tracks composing a mixed event are by construction uncorrelated, the two-particle density is then approximately equivalent to the product of single particles $\nu_1(\varphi_1)\nu_1(\varphi_2)$:

$$\nu_2^{\text{mix}}(\varphi_1, \varphi_2) \approx \nu_1(\varphi_1)\nu_1(\varphi_2). \tag{12.211}$$

This technique accounts for instrumentation effects but does not contain correlations associated with the production process. One can then obtain R_2 from the ratio

$$R_2^{\text{meas}}(\varphi_1, \varphi_2) = \frac{\nu_2(\varphi_1, \varphi_2)}{\nu_2^{\text{mix}}(\varphi_1, \varphi_2)} - 1, \tag{12.212}$$

which accounts for detection efficiencies. Indeed, given that the measured densities are

$$\nu_2(\varphi_1, \varphi_2) = \varepsilon_1\varepsilon_2\rho_2(\varphi_1, \varphi_2), \tag{12.213}$$

$$\nu_2^{\text{mix}}(\varphi_1, \varphi_2) = \varepsilon_1\varepsilon_2\rho_1(\varphi_1)\rho_1(\varphi_2), \tag{12.214}$$

one obtains the desired result

$$R_2^{\text{meas}}(\varphi_1, \varphi_2) = \frac{\rho_2(\varphi_1, \varphi_2)}{\rho_1(\varphi_1)\rho_1(\varphi_2)} - 1. \tag{12.215}$$

Similar constructions can be done for correlation analyses involving three or more particles, the study of invariant mass spectra, and essentially all types of analyses requiring a baseline or reference consisting of uncorrelated objects.

While the concept of mixed-event analysis is simple, certain precautions must be taken to avoid biases and various technical issues. For instance, in heavy-ion experiments the produced particle multiplicities are a steep function of the collision impact parameter. Considering that most instruments have an efficiency that monotonically decreases with rising detector occupancy, one must be careful to only mix events of approximately the same multiplicity and trigger type, otherwise the event mixing may result in associating incorrect efficiencies or trigger biases and thus lead to a biased measurement of cross section, or correlation function.

https://doi.org/10.1017/9781108241922.015 Published online by Cambridge University Press

Care must also be taken to mix events without carrying actual particle correlations into the synthesized mixed events. For instance, if mixed events are assembled by picking several particles from a small number of distinct events, one is effectively transposing some of the correlations that might be present in those events into the mixed events. Although the strength of these correlations is clearly diluted by event mixing, it is safest to carry out event-mixing using a single-particle per event. One must also pay attention to the fact that the number of mixed events that can be synthesized can be deceptively large. Indeed, given appropriate computing resources, it might be tempting to generate a number of mixed events far larger than the actual number of real events. Such **oversampling** of mixed events should definitely be avoided because it leads to the false impression that the efficiency correction accomplished, for instance, by calculating the normalized cumulant R_2 based on mixed events could receive no statistical error contribution from the mixed-event sample. Alas, mixed events are built from actual events. A finite number of actual events implies that single- and two-particle yields have finite statistical fluctuations. It is consequently impossible to eliminate these statistical errors and achieve mixed events with better precision than that obtained with actual events.

As a specific example, consider the generation of mixed events with a multiplicity of M particles from a pool of N events of same multiplicity M. Let us count the number of distinct mixed events that can be synthesized by randomly picking one particle per event out of M events. There are N ways to pick the first event, $N-1$ ways to pick up the second, and so on. The numbers of event combinations, $N_{\rm EC}$, is thus $N_{\rm EC} = N!/(N-M)!M!$. Since M events are sampled, there are thus M^M ways to pick up one particle per event. The resulting number of possible mixed event permutations, $N_{\rm EP}$, is thus: $N_{\rm EP} = M^M N!/[(N-M)!M!]$. For $M = 50$, and $N = 1000$, one can use the Stirling approximation to evaluate the preceding expression. One gets $N_{\rm EP} \approx 10^{150}$ which is indeed a huge number of permutations. The number can be even larger if $q > 1$ particles are picked from each event.

While the number of permutations achievable with mixed events is very large, one must realize that fluctuations of $v_2^{\rm mix}$ are also unusually large because each particle included in a mixed event is reused several times in the formation of pairs. These fluctuations were first evaluated in ref. [180] using a pair counting technique. A more direct calculation is however possible based on the realization that the synthesis of mixed events amounts to multinomial sampling. For a fixed event size M, the bin content n_i of a histogram of the density $\rho(x)$ shall have expectation values p_i, with $\sum_i^m p_i = 1$, where m is the number of bin in the histogram. The values p_i represent the probability of getting counts in each bin. Since all particles are independent because they actually originate from distinct events, the bin contents are also uncorrelated. The number of particles n_i obtain in each bin i is thus determined by a multinomial distribution.

$$P_M(n_1, \ldots, n_m | M; p_1, \ldots, p_m) = \frac{M!}{\prod_{i=1}^{m} n_i!} \prod_{i=1}^{m} p_i^{n_i}, \tag{12.216}$$

with $\sum_{i=1}^m n_i = M$. Recall from §2.10 that moments of a PDF can be calculated based on derivatives of its characteristic function. The characteristic function of a multinomial

https://doi.org/10.1017/9781108241922.015 Published online by Cambridge University Press

distribution (§3.2) is

$$\phi(t_1, t_2, \ldots, t_m) = \left(\sum_{j=1}^{m} p_j e^{it_j} \right)^n . \tag{12.217}$$

One can then readily verify (Problem 12.3) that the lower-order moments of n_i are

$$\langle n_i \rangle = \mathrm{E}[n_i] = M p_i \tag{12.218}$$

$$\langle n_i^2 \rangle = \mathrm{E}[n_i^2] = M(M-1)p_i^2 + M p_i \tag{12.219}$$

$$\langle n_i n_j \rangle = \mathrm{E}[n_i n_j] = M(M-1)p_i p_j \tag{12.220}$$

$$\begin{aligned} \langle n_i^2 n_j^2 \rangle &= \mathrm{E}[n_i^2 n_j^2] \\ &= M(M-1)(M-2)(M-3)p_i^2 p_j \\ &\quad + M(M-1)(M-2)\left[p_i^2 p_j + p_i p_j^2\right] + M(M-1)p_i p_j . \end{aligned} \tag{12.221}$$

The variance of the pair yield $n_i n_j$ expressed in terms of the averages $\langle n_i \rangle$ is thus

$$\begin{aligned} \mathrm{Var}\left[n_i n_j\right] &= \left(-\frac{4}{M} + \frac{10}{M^2} - \frac{6}{M^3} \right) \langle n_i \rangle^2 \langle n_j \rangle^2 \\ &\quad + \left(1 - \frac{3}{M} + \frac{2}{M^2} \right) \left[\langle n_i \rangle^2 \langle n_j \rangle + \langle n_i \rangle \langle n_j \rangle^2 \right] \\ &\quad + \left(1 - \frac{1}{M} \right) \langle n_i \rangle^2 \langle n_j \rangle . \end{aligned} \tag{12.222}$$

For large M, the variance of fluctuations of $n_i n_j$ thus approximately scale as $\langle n \rangle^3$. One can then write

$$\delta \langle n_i n_j \rangle \approx \langle n_i \rangle^{3/2} \approx \langle n_i n_j \rangle^{3/4} . \tag{12.223}$$

By contrast, errors on $\langle n_i \rangle$ scale as $\langle n_i \rangle^{1/2}$. We thus conclude that errors on mixed events grow faster than errors on the mean number of entries in single particle spectra. Large datasets are thus required to obtained equivalent size errors on mixed events.

Alternatively, one may also consider the number of pairs, say at specific φ_1, φ_2 values to be of the order of the product of the number of singles $n(\varphi_1)n(\varphi_2)$. Based on a full data sample, the relative error on this product, of order $n_1^{-1} + n_2^{-1}$, effects a minimum bound on the error on the number of pairs and thus two-particle densities that might be derived from them. The redeeming factor is that one is seldom interested in the density $\rho_2(\varphi_1, \varphi_2)$ directly but instead compute an average over $\bar{\varphi}$ to obtain $\rho_2(\Delta\varphi)$ which combines from one to m bins of $\rho_2(\varphi_1, \varphi_2)$. The error on the number of pairs is thus on the order or smaller than $n_1^{-1} + n_2^{-1}$. There is thus no point in generating a number of mixed events that would attempt to improve the statistical accuracy much below this bound.

12.4.6 Embedding Techniques

Embedding is a technique commonly used in experimental nuclear and particle physics to evaluate the instrumental efficiency in finding and reconstructing objects (e.g., hits, tracks,

https://doi.org/10.1017/9781108241922.015 Published online by Cambridge University Press

jets, etc.) of interest. The technique involves the insertion of tagged objects generated via MC simulations into actual events before they are reconstructed. One measures the objects' reconstruction efficiency as the degree to which they are reconstructed when embedded into actual events. This efficiency corresponds to the ratio of the number of objects N_F found by the number embedded N_E:

$$\varepsilon = \frac{N_F}{N_E}. \tag{12.224}$$

Embedding may be carried out with different levels of refinement and detail. For instance, for the evaluation of track reconstruction efficiency, one can embed tracks at the point or hit level or at the detector level, that is, in terms of simulated analog-to-digital converter (ADC) signals. While embedding points enables rapid testing of track reconstruction algorithms, it does not usually properly account for issues such as hit loss or hit overlap/merging. Full embedding simulations, for example the simulation of signal generation and propagation through the detector, is usually accomplished with the computer code GEANT with add-ons specific to each experiment. While considerably slower, full simulations make it possible to account for signal losses, interferences, merging, and so on. They thus permit as realistic as possible a simulation of the instrumental performance.

The evaluation of the error on the estimated efficiency ε requires some particular attention. Given ε is obtained from a ratio, one might at first be inclined to simply apply the quotient rule for the error on a ratio of two quantities. That would be incorrect, however, because the two quantities are not independent. In fact, by construction, the number of observed tracks is necessarily a subset of the produced or embedded tracks and one has $N_F \leq N_E$ by definition (unless there are ghost tracks). Clearly, the efficiency cannot exceed unity. One might then be inclined to use a lower limit only if the ratio is near unity, or a two sided error interval if the estimated efficiency is considerably smaller than unity. This amounts to flip-flopping, as discussed in §6.1.8. Fortunately, the unified approach introduced in §6.1.8 alleviates this problem and enables the definition of error intervals without flip-flopping or empty intervals, and no undercoverage. Its application for binomial sampling, relevant for efficiency estimates by embedding and related techniques, is discussed in §6.2.2.

12.4.7 Closure Test

Data correction methods can get pretty involved and complicated. But just because sophisticated unfolding techniques promise properly corrected data does not mean they deliver precise and unbiased results. It is thus useful to carry out a **closure test**.

The basic idea of a closure test is quite simple: (1) define a parent distribution f_P that mimics or might closely resemble the actual distribution; (2) produce a large number of events on the basis of this distribution and process them through a performance simulator of the experiment, its event reconstruction software, and the data analysis to obtain a simulated raw distribution f_{raw}; (3) proceed to unfold or correct the raw data to obtain a corrected (unfolded) distribution f_{corr}; (4) compare the unfolded distribution f_{corr} with

https://doi.org/10.1017/9781108241922.015 Published online by Cambridge University Press

the original distribution f_P to verify whether the unfolding procedure yields an unfolded distribution statistically compatible with the parent distribution.

Comparison of the f_{corr} and f_P distributions may begin with a simple visual inspection. It should be possible to instantly recognize improperly unfolded data if the two distributions deviate significantly from one another. However, given finite computing resources, the distributions shall have finite statistical errors, and it may not be visually obvious whether the distributions are in fact in mutual agreement, or not. It is then necessary to make use of a statistical test (§6.4). The null hypothesis of this test shall be that the unfolded distribution f_{corr} is undistinguishable from the parent distribution f_P. The test may then be implemented as a histogram compatibility test (§6.6.6) or Kolmogorov–Smirnov test (§6.6.7) using a predetermined significance level β. The significance level shall be chosen, based on the desired level of experimental accuracy, to minimize the risk of an error of the second kind, that is, to falsely accept the null hypothesis and consider the corrections are properly carried out when in fact they are not.

12.5 Systematic Errors

12.5.1 Definition

Systematic errors are measurements errors associated with the "system," that is, the measurement technique, the experimental protocol, or the analysis method used to carry out a measurement. Unlike statistical errors, which can be arbitrarily reduced in magnitude by repeating measurements of a specific phenomenon, statistical errors are an intrinsic flaw of the "system" and thus cannot be reduced or eliminated by repeating a measurement. Indeed, nothing is gained by repeating a flawed procedure several times. Systematic errors are due to biases introduced by the measurement technique or protocol. Since a bias does not disappear when a measurement is repeated, there is, in fact, no point in repeating the same measurement many times. The bias will persist, and the repeated measurements will have small statistical errors and thus might give the illusion that the results are accurate and precise. However, while increased statistics improve the precision of a measurement, the measurement remains inaccurate because it is systematically biased. Measured values tend to be consistently either to small or too large and having a zillion data points cannot fix that basic problem. This said, having a large data sample may enable a careful and detailed analysis which might unravel the presence of biases. But at the end of the day, understanding biases and systematic errors requires one has an in-depth understanding of all aspects of a particular measurement.

12.5.2 The Challenge

Systematic errors often affect (but not always) all data points of a particular measurement in a similar way: all points tend to be either too low or too large. For instance, consider a measurement of distances made with a stretched out tape measure. If the fabric or material

https://doi.org/10.1017/9781108241922.015 Published online by Cambridge University Press

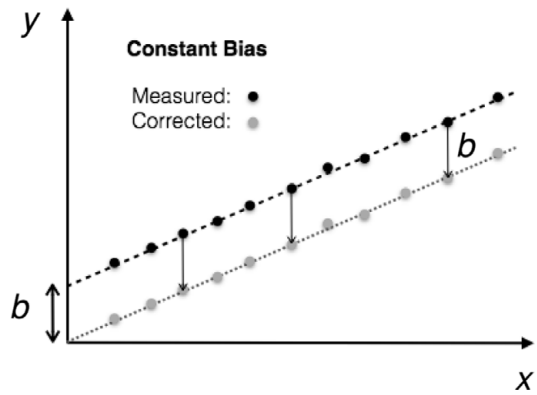

Fig. 12.12 Correcting for constant bias is possible if a signal can be measured, or extrapolated as shown, at a point where the magnitude is null or known to have a specific value by definition or construction. Here, the signal is expected to be null at $x = 0$; one can then use the observed offset b as an estimate of the measurement bias to correct all data points.

of the tape measure is worn out and stretched due to repeated usage or improper handling, distances or sizes measured will appear consistently smaller than they really are no matter what the size or distance is. The measured distances will thus be systematically too small. However, when measuring functional dependencies, for instance, $y \equiv y(x)$, one may find that the bias on y may itself be a function of x and y. The bias might indeed tend to be larger (or smaller) for a certain range of values of either x or y, and it might in fact be an arbitrarily complicated function of either variables.

Constant biases are least problematic. Indeed, if a bias δy_{bias} can be identified at specific value of x, and one has good reasons to believe it is constant for all values of x, than measured values $y(x)$ can be corrected for by subtracting the identified bias from all measured values:

$$y_{\text{corrected}} = y_{\text{measured}} - \delta y_{\text{bias}}. \tag{12.225}$$

This situation arises when the signal y is expected to be null, by construction or by definition, for a specific value of x. For instance, if one expect y to be strictly proportional to x and null for $x = 0$, one can detect the presence of a bias, as illustrated in Figure 12.12, by extrapolating measured data points to the origin, $x = 0$. Unfortunately, systematic errors are not always obvious or constant, and a lot of "digging" may be required to identify their presence and approximate magnitude. Failure to identify and correct for systematic biases may have consequences ranging from mild inconvenience to catastrophic failure and erroneous scientific conclusions.

The biggest problem with systematic biases is that it is usually not possible to precisely determine the magnitude or the functional dependence of the bias. Indeed, it is one thing to identify the presence of a source of bias, but it is usually a bigger challenge to determine the magnitude of the effect. One is thus required to make "educated" guesses as to what the magnitude of the biases might be and how they could impact the measured data. In the end, one is forced to acknowledge that the "final" data might be over- or undercorrected for biases. One must then estimate the range of one's ignorance (minimum and maximum

https://doi.org/10.1017/9781108241922.015 Published online by Cambridge University Press

corrections possible and consistent with the experimental method and the measured data) on the proper magnitude of corrections and determine how such uncertainties impact the corrected data. The range of applicable corrections then determines a range of measured values that one can quote as systematic errors when reporting the measured data.

As a specific example, let us consider the fixed bias correction illustrated in Figure 12.12. Here, the presence of a bias is readily identified because the signal y is expected to vanish at $x = 0$ but manifestly does not. One uses the extrapolated signal at $x = 0$ to estimate the bias b and correct all data points (gray dots). While straightforward, this correction procedure entails several issues. First, the extrapolation to the origin is only as good the linear fit to the data points. If the statistic is poor, the extrapolated value $y(0)$ may be arbitrarily large or small, and the corrected data shall correspondingly be too low or too high. Second, this procedure assumes the data is strictly governed by a linear dependence. What if, in fact, the phenomenon has a quadratic (or higher order) dependence on x? The extrapolation would then most likely be wrong and so would the corrected data. And third, it is also possible that while the linear model is correct, various instrumental effects may cause an artificial higher-order polynomial dependence of the signal y on x (in other words, the bias depends on x). Use of a linear extrapolation would once again produce an incorrect (or at the very least incomplete) correction. The task of the experimentalist is thus to evaluate, to the best of their ability, the magnitude of such effects. The error on b (which is subsequently subtracted from all data points) obtained from a linear would constitute a first estimate of systematic errors on the data points. One could also use higher-order (nonlinear) fits to extrapolate to the origin and possibly enlarge the range of the offset b consistent with the data, and which is subtracted to obtain corrected data.

The preceding example is rather simplistic. In practice, the presence of biases may not be obvious and evaluating the magnitude of known systematic effects is not a trivial matter. In fact, it is often the case that far more time and efforts are spent understanding and evaluating systematic errors than carrying out the measurement in the first place. It is also the case that the challenge of the task typically increases in proportion to the accuracy one wishes to achieve in a particular measurement.

12.5.3 Reporting and Improving Errors

Statistical and systematic errors have distinct causes and origins. It has thus become common practice, in most scientific disciplines, to report measurements with statistical and systematic error bars independently. This enables an explicit acknowledgment of the precision and accuracy achieved in the reported measurement. Assuming the statistical estimator used to determine the reported parameters are unbiased (or asymptotically unbiased but with a very large dataset), the statistical error bars provide an indication of the level of precision achieved in the measurement, while the systematic errors indicate the estimated level of accuracy. It is then possible to evaluate, at a glance, the merits of an experiment and identify its weaknesses. Experiments are said to be **statistics limited** if the statistical error bars are larger, for the most part, than systematic errors. Conversely, if the latter predominate, the experiment is described as **systematics limited**.

https://doi.org/10.1017/9781108241922.015 Published online by Cambridge University Press

Achieving a better statistical error is conceptually simple, it suffices to significantly increase the size of the data sample. In particle and nuclear physics experiments, this can be achieved by increasing the duration of the experiment, the intensity of the beam and target thickness (the luminosity of the machine), the acceptance, or detection efficiency of the apparatus. Improving on a systematic limited experiment can be significantly harder. One must indeed achieve better control over the various biases and improve on the techniques used to suppress or correct for these biases. Such improvements typically require novel experimental techniques or better ways to analyze the data.

12.5.4 Brief Survey of Sources of Systematic Errors

Sources of systematic errors are as varied as the observables and measurements techniques used in experimental physics. It is consequently not possible to provide an exhaustive list of all types of systematic errors that may arise in practice. At the outset, it is quite important to have a good understanding of the experimental apparatus, the measurement protocol, as well as the properties and limitations of the observables under study. Indeed, only a careful examination of the properties and attributes of the detector components and analysis techniques used in a measurement of interest may reveal sources of biases and systematic errors. Nevertheless, one may formulate a few generic remarks about the process of understanding systematic errors and their most common sources.

As we have discussed at great length in this and earlier chapters, scientific measurements involve a large number of steps and operations, each of which is susceptible of introducing some kind of bias or systematic error. Two broad classes of systematic errors are worth considering. The first class involves sources of errors associated with the measurement itself whereas the second is concerned with "physical backgrounds."

Measurement Biases

The reconstruction of events and measurements of cross sections in nuclear (or elementary particle) scatterings involve several steps, including signal calibration, correction for detection efficiencies and experimental acceptance, as well as signal smearing (resolution effects). Each of these may indeed contribute a source of bias and systematic errors.

The calibration of energy and timing signals typically involves the subtraction of an ADC (TDC) pedestal and multiplication by an appropriate gain factor. Pedestals and gains are determined by experimental procedures and protocols which may be statistic or systematic limited (§9.1.3). They are thus known with finite precision and accuracy. They may also change over time for a variety of reasons. The pedestals and gains used in an analysis may then be slightly off, and induce biases in the energy (amplitude) or time scales of the measurement. This is particularly the case, for energy measurements, when the reference used to obtain the gain calibration lies at much lower energy than typical energy signals of interest in the physical measurement. The signal gain calibration is then effectively based on an extrapolation, which may result in gross under- or overestimation of the measured amplitudes, energies, or timing signals. Additional issues may arise if nonlinearities are

https://doi.org/10.1017/9781108241922.015 Published online by Cambridge University Press

involved in the energy or charge collection process. Together, these effects introduce a systematic uncertainty on the energy (charge, amplitude, or time) scale of the measurement.

Most measurements carried out in particle and nuclear physics involve some form of counting. For instance, one associates and counts hits to form tracks, tracks to form events, which may, in turn, also be counted. All these counting steps are predicated on some quality control cuts: not all produced objects (e.g., hits, charged particle track, energy shower, collision event, etc.) are duly counted and an arbitrary fraction may be missed. It is the purpose of efficiency (and acceptance) corrections to account for these losses. Obviously, although many distinct techniques might be used to estimate detection efficiencies, there remains the possibility that efficiencies may be, as for gains, under- or overestimated. Such uncertainties may arise for a variety of reasons, including the finite size of data samples, simulation samples, as well as improper characterization or modeling of the measurement process. Together, these effects lead to systematic uncertainties on the magnitude of cross sections.

Measurement errors affecting both the energy scale and the magnitude of the cross section may also arise due to finite resolution or signal smearing, whether unfolded or not. For instance, momentum or energy smearing of a steeply falling cross section spectrum (i.e., with increasing momentum) has a tendency to spread cross sections from low to high momenta, thereby disturbing the functional shape of the cross section dependence on energy or momentum.

Systematic uncertainties on cross sections may also arise because of faked (often called ghost) objects, most particularly tracks. For example, faked hits may be produced by noisy detector signals and lead to random associations of hits into faked or improperly measured tracks. Faked or ghost tracks may then end up being counted as real tracks and artificially inflate the measured cross sections. Ghost tracks are most common at low momenta because spurious hits are more easily associated to large curvature tracks than straight tracks.

Various other forms of **pile-up** may occur and lead to biases. An obvious example of pile-up involves the detection of tracks from several distinct collisions in slow detectors such as time projection chambers. Tracks from different collisions may appear unresolved and result in apparent high-multiplicity events, thereby shifting the production cross section from low to high multiplicity.

Biases may also occur because of the physical processes involved in the detection and measurement of signals. For instance, charged particles lose energy as they penetrate through the various materials composing a detector. Energy losses imply a reduction in momentum, which in turn results in an increase of curvature for charged particle tracks. The track energy loss thus introduces a small downward bias in the moment of particles, which cannot, typically, be compensated for equally well for all particle masses or species. Since energy losses are largest in the $1/\beta^2$ regime, this results in a slight distortion of the energy scale, which typically affects low momenta the most.

Event triggering (i.e., the selection of events with particular features), whether performed with actual triggering detectors, or in software during the data analysis may also induce various forms of biases, most particularly on the efficiency and cross section of processes. For instance, requiring that a scattering event contains one or two high-energy jets tends to skew the event multiplicity distribution toward high-multiplicity values. It

https://doi.org/10.1017/9781108241922.015 Published online by Cambridge University Press

obviously also affects the measured momentum distribution. Scattering measurements are often recorded with **minimum-bias** triggers. These are typically based on large detector arrays capable of detecting a sizable fraction of the produced particles. They are usually designed to collect all inelastic collisions with uniform efficiency and irrespective of the produced particle multiplicity. In practice, the finite size and limited efficiency of these detectors results in cross section biases, most particularly for low-multiplicity events. There is thus no such a thing as a truly unbiased minimum-bias trigger.

Physical Backgrounds

Physical backgrounds may also constitute sources of biases, particularly in measurements of cross sections. They can be broadly be divided into two classes. The first class consists of physical processes taking place within the detector because of electromagnetic or hadronic interactions of produced particles (i.e., particles produced by the scattering under study) with materials of the detector, while the second involves processes produced directly by the collision under study (i.e., irrespective of the presence of a detector).

At the outset of this discussion, recall the notions of primary, secondary, and tertiary tracks that we introduced in §8.3.1. Primary tracks are those tracks that are produced at the primary vertex of an interaction whereas secondary tracks originate from decays of primary particles as they traverse the detection apparatus. We have called tertiary tracks those tracks that are produced by interaction (electromagnetic or hadronic) of primary and secondary particles with materials of the detector. Experimentally, the segregation of primary, secondary, and tertiary tracks (particles) is largely based on their distance of closest approach to the primary vertex of an interaction. However, by virtue of the stochastic nature of decays and interaction with materials, secondary and tertiary particles may occur at arbitrarily small distances from the primary vertex and thus be indistinguishable, in practice, from primary particles. Secondary (and tertiary) particles produced near the vertex thus constitute a background in the determination of primary particle production cross section. Conversely, because finite resolution effects smear the DCA of tracks, primary tracks may appear as secondary tracks and thus contribute a sizable combinatorial background in the identification of decaying particles via topological cuts or invariant mass reconstruction (§8.5.1). Similarly, tertiary tracks may also be mis-identified as either primary or secondary tracks and thus constitute a source of background (and cross section bias) for these particle types. Cross contamination of primary and secondary (as well as tertiary) is typically based on distance of closest approach (DCA) cuts. Tight (short) maximum DCA cuts are required to select primary and reject secondary tracks whereas wide minimum DCA cuts are used to select secondary particles. No matter what cut values are used, however, some secondary tracks end up being selected as primary particles, and some primary particles are categorized as secondary. This unavoidable misidentification of the two types introduces backgrounds and thus biases in cross section measurements of both types of particles, and although these biases can be suppressed to some degree by judicial DCA cuts, they can never be eliminated. It is thus a common feature of all cross section analyses to study particle yields as a function of DCA cut values in order to estimate the relative contributions of the two types of particles. Unfortunately, such studies cannot be performed with perfect

https://doi.org/10.1017/9781108241922.015 Published online by Cambridge University Press

accuracy and one is thus required to include systematic errors on particle yields (or cross sections) based on trends and extrapolations.

Contamination from secondary particles is particularly insidious for measurements of correlation functions. Secondary particles produced by two- or three-body decays are de facto correlated by virtue of energy-momentum conservation. They thus naturally produce spurious correlation features in two- (or three-) particle correlation functions. As for measurements of single particle cross sections, one can use DCA cuts to reduce or suppress the impact of these spurious correlation features but they cannot be completely eliminated. One must then resort to systematic studies of the strength and shape of the correlation functions when DCA cuts are changed. It then becomes possible to report systematic errors on the amplitude of the correlation functions.

Various other physical and detector induced processes produce backgrounds in single particle cross section measurements and spurious features in two- or three-particle correlation functions. Particularly important in measurements of correlation functions are processes of pair creation by photons as they interact electromagnetically with high atomic number materials of a detector. Pair creation produces a forward going pair of positron and electron which result in a sharp peak at the origin of $\Delta\eta - \Delta\phi$ correlation functions of unlike-sign charged particle pairs. This type of contamination may be suppressed by rejecting electron-like particle signals (e.g., based on dE/dx, TOF, or Cerenkov radiation) and a minimum cut on the invariant mass of the pair (since pair conversion tend to produce a very low mass peak). Contamination may persist and it is thus necessary to assess systematic effects on correlation functions associated with these conversions.

Biases in measurements of single particle correlation and correlation functions may also arise because of track splitting and track merging (defined in §12.4.3). Track splitting leads to an artificial increase of the cross section and spurious correlation features at small $\Delta\eta$ and $\Delta\phi$ values. It can usually be suppressed significantly by requiring "long" tracks, that is, tracks that contain at least 50% of possible hits. Splitting contamination may remain, however, in spite of cuts, and it is necessary to estimate track splitting effects, for instance, by varying the minimum number of hits requirement.

Track merging poses a more serious difficulty. Indeed, the crossing of tracks with similar pseudorapidity and azimuth of production yields merged or unresolved hits which, in turn, lead to the reconstruction of fewer track pairs. One is then faced with a difficult loss of single and particle-pair to evaluate. These result in a reduction of the single particle cross section and a loss of particle pairs at small $\Delta\eta - \Delta\phi$ values. Such losses can in principle be modeled with Monte Carlo simulations. In practice, the accuracy of this type of simulations is severely limited by complicated and changing response features of particle detectors. One is then required, once again, to estimate systematic effects associated with the loss of particles, and most particularly pairs of particles produced at small relative pseudorapidities and azimuthal angles.

The aforementioned effects are the most common and salient effects encountered in measurements. However, many other effects may need to be considered in practical situations, such as loss of signals or spurious noise associated with various types of detector malfunction.

https://doi.org/10.1017/9781108241922.015 Published online by Cambridge University Press

Exercises

12.1 Use an arbitrary Fourier decomposition of the efficiencies $\varepsilon(x_i)$ and the correlation function R_2 to demonstrate that Eq. (12.181) yields a robust result, i.e., is independent of efficiencies. Verify that is not the case for coordinates without periodic boundary conditions (e.g. $\Delta\eta$).

12.2 Verify Eq. (12.203) expressing the robustness measure $\xi(x_1, x_2)$.

12.3 Use the characteristic function $\phi(t_1, t_2, \ldots, t_m)$ of the multinomial distribution given by Eq. (12.217) to derive the lowest order moments of the distribution listed in Eqs. (12.218–12.221).

12.4 Show that $\frac{\partial \chi^2(\vec{\mu})}{\partial \mu_k} = 0$ is satisfied by Eq. (12.37).

12.5 Derive the expression of the covariance matrix U_{ij} given by Eq. (12.55).

12.6 Show that all singular values of an orthogonal matrix $\mathbf{A}$ are equal to unity.

12.7 Verify that the estimator (12.37) corresponds to the solution obtained by maximization of the log-likelihood function and yield

$$\log L(\mu) = \sum_{i=1}^{N} \log\left(P(n_i|\nu_i)\right),$$

where $P(n_i|\nu_i)$ is a Poisson distribution (or binomial distribution).

https://doi.org/10.1017/9781108241922.015 Published online by Cambridge University Press